HHS Public Access

Author manuscript

Nature. Author manuscript; available in PMC 2022 June 09.

Published in final edited form as:

Nature. 2021 October ; 598(7882): 641–645. doi:10.1038/s41586-021-04001-4.

A neuroanatomical basis for electroacupuncture to drive the vagal-adrenal axis

Shenbin Liu[#,1,2,3,4], **Zhifu Wang**[#,1], **Yangshuai Su**[1,5], **Lu Qi**[1], **Wei Yang**[1], **Mingzhou Fu**[1], **Xianghong Jing**[5], **Yanqing Wang**[2,3,4], **Qiufu Ma**[6]

[1]Dana-Farber Cancer Institute and Department of Neurobiology, Harvard Medical School, Boston, MA, USA.

[2]Institute of Acupuncture and Moxibustion, Fudan Institutes of Integrative Medicine, Fudan University, Shanghai, China.

[3]Department of Integrative Medicine and Neurobiology, School of Basic Medical Science, Fudan University, Shanghai, China.

[4]State Key Laboratory of Medical Neurobiology, Institutes of Brain Science, Fudan University, Shanghai, China.

[5]Meridians Research Center, Institute of Acupuncture and Moxibustion, China Academy of Chinese Medical Sciences, Beijing, China.

[6]Dana-Farber Cancer Institute and Department of Neurobiology, Harvard Medical School, Boston, MA, USA.

Summary

Somatosensory autonomic reflexes allow electroacupuncture stimulation (ES) to modulate body physiology at distant sites[1-6] (for example, suppressing severe systemic inflammation[6-9]). Since the 1970s, an emerging organizational rule about these reflexes has been the presence of body-region specificity[1-6]. For example, ES at the hindlimb ST36 acupoint but not the abdominal ST25 acupoint can drive the vagal–adrenal anti-inflammatory axis in mice[10,11]. The neuroanatomical basis of this somatotopic organization is, however, unknown. Here we show that PROKR2^{Cre}-marked sensory neurons, which innervate the deep hindlimb fascia (for example, the periosteum) but not abdominal fascia (for example, the peritoneum), are crucial for driving the vagal–adrenal axis. Low-intensity ES at the ST36 site in mice with ablated PROKR2^{Cre}-marked sensory neurons failed to activate hindbrain vagal efferent neurons or to drive catecholamine release

Correspondence and requests for materials Should be addressed to Qiufu Ma: Qiufu_Ma@dfci.harvard.edu.
[#]Contributed equally.

Author contributions

S.L. and Z.W. jointly performed most experiments. Y.S. helped to determine electric stimulation intensities for driving distinct autonomic pathways. L.Q. helped to characterize the identities of PROKR2^{Cre}-marked sensory neurons. W.Y. determined differential representations of PROKR2^{Cre}-marked DRG neurons at differential axial levels, and M.F. helped to show innervation of PROKR2^{Cre}-marked sensory neurons in fascial tissues. Q.M. conceptualized and supervised the entire study (with contributions from Y.W. and X.J.). S.L. and Q.M. wrote the manuscript, and all authors edited the manuscript.

Reporting summary

Further information on research design is available in the Nature Research Reporting Summary linked to this paper.

Competing interests

The authors declare no competing interests.

from adrenal glands. As a result, ES no longer suppressed systemic inflammation induced by bacterial endotoxins. By contrast, spinal sympathetic reflexes evoked by high-intensity ES at both ST25 and ST36 sites were unaffected. We also show that optogenetic stimulation of PROKR2^{Cre}-marked nerve terminals through the ST36 site is sufficient to drive the vagal–adrenal axis but not sympathetic reflexes. Furthermore, the distribution patterns of PROKR2^{Cre} nerve fibres can retrospectively predict body regions at which low-intensity ES will or will not effectively produce anti-inflammatory effects. Our studies provide a neuroanatomical basis for the selectivity and specificity of acupoints in driving specific autonomic pathways.

A core idea of acupuncture to treat human diseases is that stimulation at specific body regions (acupoints) can modulate body physiology at distant sites, an effect that is thought to operate through hypothetical meridian channels. Although modern anatomical studies have not yet supported the physical presence of such channels[12], long-distance acupuncture effects can be achieved through somatosensory autonomic reflexes. These reflexes start with the activation of peripheral nerves derived from neurons located in dorsal root ganglia (DRG) and/or trigeminal ganglia followed by the transmission of sensory information from the spinal cord to the brain, the subsequent activation of peripheral autonomic pathways and the eventual modulation of various aspects of body physiology[2-6]. For this study, the goal was to investigate why ES can drive the recently reported vagal–adrenal axis from the hindlimb Zusanli (ST36) acupoint but not from the abdominal Tianshu (ST25) acupoint, at which ES instead drives spinal sympathetic reflexes[10,11] (Fig. 1a). We postulated that somato–vagal–adrenal reflexes are driven by sensory pathways that innervate tissues unique to the hindlimbs compared to the abdomen, such as joints, bones and skeletal muscles. One candidate pathway includes DRG neurons marked by PROKR2^{Cre} (in which with Cre-mediated recombination marks neurons with persistent or transient expression of prokineticin receptor 2[13]). These neurons innervate deep limb tissues but not skin epidermis[13].

Fascia innervation by PROKR2^{Cre} neurons

To characterize PROKR2^{Cre} neurons, we generated *Prokr2^{Adv}-tdTomato* mice, in which the tdTomato reporter was restricted to DRG neurons defined by the developmental co-expression of PROKR2^{Cre} (ref. [13]) and Advillin^{Flpo} (ref. [14]) (Extended Data Fig. 1a). PROKR2^{ADV}-tdTomato^{+} cells were detected in a subset of DRG neurons (Fig. 1b, c), but not in sympathetic ganglia, adrenal glands or enteric ganglia, and were rarely seen in nodose ganglia (Extended Data Fig. 1b). Notably, PROKR2^{ADV} DRG neurons had higher representations at limb levels than at thoracic levels (Extended Data Fig. 2a, b), with 16.7 ± 1.4% (mean ± s.e.m.) of TUBB3^{+} neurons co-expressing tdTomato in L4–L5 lumbar DRGs compared with 6.1 ± 0.3% in T8–T10 thoracic DRGs (Fig. 1b, c). Within lumbar DRGs, PROKR2^{ADV} neurons did not overlap with IB4-binding non-peptidergic neurons, which innervate skin epidermis[15], or parvalbumin-expressing proprioceptors (Extended Data Fig. 1c). Among tdTomato^{+} neurons, 82.9 ± 1.2% co-expressed the nerve growth factor receptor TRKA, 57.2 ± 1.8% co-expressed the neurofilament protein NEFH, 63.9 ± 3.6% co-expressed the calcitonin gene-related peptide (CGRP) and 50.7 ± 3.9% co-expressed NEFH plus CGRP (Extended Data Fig. 1c). Furthermore, *Nefh* mRNA expression levels

showed that *Nefh*$^{+}$tdTomato^{+} neurons were divided into *Nefh*^{high} and *Nefh*^{low} subtypes. The *Nefh*^{high} subset represented 7.5 ± 0.8% of TUBB3^{+} neurons in L4–L5 DRGs, which is more than three times the number seen in T8–T10 DRGs (2.0 ± 0.1%) (Fig. 1b, c). By contrast, the *Nefh*^{low} subset did not show any marked representation difference in lumbar (2.7 ± 0.3%) versus thoracic (2.1 ± 0.2%) DRGs (Fig. 1b, c). Thus, *Nefh*^{high} PROKR2^{ADV} neurons are enriched in limb-level DRGs.

We next characterized innervation patterns. Centrally, PROKR2^{ADV} neurons mainly innervated superficial laminae of the dorsal spinal cord, whereas deep laminae were innervated to a lesser extent (Extended Data Fig. 2c, d). Peripherally, for both hindlimb and abdominal regions, tdTomato^{+} fibres did not innervate skin epidermis but formed circumferential endings around hair follicles. These endings showed strong CGRP expression without detectable NEFH protein expression (Extended Data Fig. 3b, c). Nearly all tdTomato^{+} neurons that were retrogradely labelled from the skin co-expressed *Bmpr1b* and low levels of *Nefh* mRNA (Extended Data Fig. 3d, e), representing the CGRP-ε subtype of Aδ nociceptors[16-18]. By examining innervation in deep tissues, we found a body-region difference. In the hindlimb, tdTomato^{+} fibres densely innervated fascial tissues, including the periosteum, joint ligaments and the interosseous membrane between the tibia and the fibula (Fig. 1d, Extended Data Fig. 4a-c). A total of 63.5 ± 4.1% of periosteum-innervating tdTomato^{+} fibres co-expressed NEFH and CGRP (Extended Data Fig. 4d). NEFH^{+}tdTomato^{+} fibres also abundantly innervated the inner compartment of the tibialis anterior (TA) muscle, in a space that probably corresponds to fascia wrapping muscle bundles (Extended Data Fig. 4e). PROKR2^{ADV}-tdTomato^{+} neurons accounted for 38.7 ± 1.3% of neurons retrogradely labelled from the deep ST36 tissue. Among them, 75.6 ± 1.3% co-expressed high levels of *Nefh* mRNA, and only 10.6 ± 1.0% co-expressed *Bmpr1b* and 12.5 ± 1.0% low levels of *Nefh* mRNA (Extended Data Fig. 4f, g). This expression profile distinguished them from *Bmpr1b*$^{+}$ *Nefh*^{low} PROKR2^{ADV}-tdTomato^{+} neurons that innervate hair follicles. In contrast to dense innervation in deep hindlimb fascia, tdTomato^{+} fibres were not detected in the peritoneum, which is the major deep fascia in the abdomen (Fig. 1e). Notably, compared with the inner TA at the ST36 site, tdTomato^{+} fibre densities were tenfold lower in the outer TA or in abdominal wall muscles at the ST25 site (Extended Data Fig. 4h), which echoes the developmental and functional segregation between the two TA compartments[19]. Thus, the unique innervations to deep fascial tissues by NEFH^{high}tdTomato^{+} neurons offer a way to distinguish the hindlimb ST36 region from the abdominal ST25 region (Extended Data Fig. 4i, j).

Necessity for driving the vagal–adrenal axis

To study the functions of PROKR2^{ADV} neurons, we generated *Prokr2*^{Adv}*-DTR* mice, in which the expression of the diphtheria toxin (DTX) receptor (DTR) was restricted to PROKR2^{ADV} DRG neurons (Extended Data Fig. 5a, b). Four weeks after DTX injections, 98.0 ± 0.5% of PROKR2^{Cre}-marked DRG neurons were ablated (Extended Data Fig. 5c), which led to 44.5 ± 7.0% and 72.4 ± 5.7% reductions in TUBB3^{+} and NEFH^{+} fibre densities, respectively, in the periosteum (Extended Data Fig. 5d). Notably, no ablation was observed in the spinal cord or brain (Extended Data Fig. 5e). We refer to these mice as PROKR2^{ADV}-Abl.

To determine whether PROKR2^{ADV} neurons drive the vagal–adrenal axis, we performed ES of the hindlimb ST36 acupoint (Fig. 2a). Pairs of electric needles were bilaterally inserted into TA muscles, with tips close to the peroneal nerves (Fig. 2a, Extended Data Fig. 3a). In control mice, low-intensity (0.5 mA) ES was sufficient to induce Fos expression, a marker for neuronal activation, in hindbrain vagal efferent neurons located in the dorsal motor nuclei of the vagus (DMV) and marked by the expression of choline acetyltransferase (ChAT) (Fig. 2b). This Fos induction was eliminated in PROKR2^{ADV}-Abl mice (Fig. 2b). A 0.5-mA ES of the ST36 site can cause release of noradrenaline, adrenaline and dopamine from adrenal chromaffin cells that is dependent on the vagal nerve[10,11]. Such release was virtually eliminated in PROKR2^{ADV}-Abl mice (Fig. 2c), which indicates that PROKR2^{ADV} neurons have a role in activation of the vagal–adrenal axis by low-intensity ES.

Activation of the vagal–adrenal axis can suppress systemic inflammation induced by lipopolysaccharide (LPS), a bacterial endotoxin[10,11,20]. Without LPS treatment, proinflammatory cytokines, including tumour necrosis factor (TNF) and interleukin-6 (IL-6), were barely detected in serum (Extended Data Fig. 6a). In LPS-treated control littermates, 0.5-mA ES at the ST36 site caused a 50% reduction in TNF and IL-6 induction and a 40% increase in survival rates compared with sham ES, and these effects were abolished in PROKR2^{ADV}-Abl mice (Fig. 2d-g). We have previously reported11 that 0.5-mA ES of the abdominal ST25 acupoint does not drive vagal or sympathetic reflexes and is unable to suppress systemic inflammation. High-intensity ES of the ST25 site can drive sympathetic reflexes and produce weak (through 1.0-mA ES) or strong (through 3.0-mA ES) anti-inflammatory effects independent of vagal efferents[11]. These effects were unchanged in PROKR2^{ADV}-Abl mice (Extended Data Fig. 6b-j). High-intensity (3.0-mA) ES of the hindlimb ST36 acupoint also drove spinal sympathetic reflexes and produced anti-inflammatory effects independent of PROKR2^{ADV} neurons (Extended Data Fig. 7a, b). Thus, PROKR2^{ADV} neurons are uniquely required for low-intensity ES to drive the vagal–adrenal anti-inflammatory axis from the hindlimb ST36 acupoint.

Sufficiency for driving the adrenal axis

We next performed gain-of-function studies by generating *Prokr2^{Adv}-CatCh* mice, in which the expression of the calcium-translocating channelrhodopsin (CatCh)[21] plus the enhanced yellow fluorescent protein (eYFP) reporter was confined to PROKR2^{ADV} neurons (Extended Data Fig. 8a). eYFP^{+} neurons were detected in DRGs and showed innervations in the periosteum (Extended Data Fig. 8b, c). Electrophysiological recordings demonstrated that blue-light pulses evoked action potential firing in a subset of DRG neurons from *Prokr2^{Adv}-CatCh* mice, but none in control littermates (Extended Data Fig. 8d, e).

We then performed opto-acupuncture by inserting optic fibres bilaterally into the inner TA through the ST36 sites (Fig. 3a). Blue-light stimulation failed to drive sympathetic reflexes (Extended Data Fig. 8f, g), and we accordingly focused on vagal reflexes. Previous studies have revealed spinal ascending projections to the solitary tract nuclei (NTS) in the medulla oblongata, which send outputs to the DMV[22,23]. Optical stimulation of the ST36 site increased Fos induction in lamina I spinal neurons retrogradely labelled from NTS from 3.3 ± 0.9% in control littermates to 52.7 ± 7.1% in *Prokr2^{Adv}-CatCh* mice

(Extended Data Fig. 9a, b). Moreover, induction of $ChAT^{+}$ vagal efferent neurons within the DMV was increased from 10.8 ± 1.4% in control mice to 30.2 ± 1.8% in Prokr2Adv-CatCh mice (Fig. 3b). Consistently, electrophysiological recordings in the left cervical vagal nerve (Extended Data Fig. 8g) showed a 15-fold increase in discharge rates in response to bilateral optical stimulation of the ST36 site (Fig. 3c). Meanwhile, blue-light stimulation of the ST36 acupoint caused an increase in serum levels of noradrenaline, adrenaline and dopamine in *Prokr2*^{Adv}*-CatCh* mice compared with control littermates (Fig. 3d). This increase was eliminated after subdiaphragmatic vagotomy (Fig. 3d). As circulating adrenaline and dopamine are mainly from the adrenal glands[10,11], these data suggest that activation of $PROKR2^{ADV}$ neurons sufficiently drives the vagal–adrenal axis. Consistently, blue-light stimulation of the ST36 site caused an increase in Fos induction in vagal efferent neurons retrogradely labelled from adrenal glands (from 12.1 ± 2.3% in control littermates to 47.7 ± 3.7% in *Prokr2*^{Adv}*-CatCh* mice; Extended Data Fig. 9c, d). Moreover, blue-light stimulation of the ST36 acupoint caused a 50% reduction in TNF and IL-6 production and a 50% increase in survival rates in LPS-treated *Prokr2*^{Adv}*-CatCh* mice compared with control mice (Fig. 3e-g, Extended Data Fig. 9e). This anti-inflammatory effect was lost after subdiaphragmatic vagotomy (Fig. 3e, f). Thus, optical activation of $PROKR2^{ADV}$ fibres essentially mimics 0.5-mA ES of ST36 and can sufficiently drive the vagal–adrenal anti-inflammatory axis.

Involvement of deep limb fascial nerves

$PROKR2^{ADV}$ neurons innervate both cutaneous and deep tissues, with the *Nefh*^{low}*Bmpr1b*$^{+}$ subset innervating hair follicles in a region-independent manner and the *Nefh*^{high} neurons preferentially innervating hindlimb fascial tissues (Extended Data Fig. 4i, j). To achieve body-region specificity, vagal reflexes may be evoked by the common peroneal nerve, which contains fibres innervating deep fascia, rather than by the lateral cutaneous nerve, which innervates the skin[24]. To test this hypothesis, we generated mice with selective transection of the common peroneal nerve or the lateral cutaneous nerve (referred to as CPX and CLX, respectively), plus control mice that underwent sham surgery (Fig. 4a). In CPX mice, focal electric stimulation and insertion of needles to 3-mm depth eliminated the suppression of TNF and IL-6 production induced by 0.5-mA ES at the ST36 site, with selective loss of innervation in the bone periosteum and deep muscles at the anterior side. This effect was not observed in mice in which transection of the tibial nerve was located posterior to the fibula and the tibia (Fig. 4b, c, Extended Data Fig. 10a), even though tibial nerve activation, evoked through a diffuse ST36 ES mode, can redundantly produce anti-inflammatory effects[10]. Consistently, Fos induction in NTS-projecting spinal neurons evoked by a focal 0.5-mA ES at the ST36 site was eliminated in CPX mice (Extended Data Fig. 10b). By contrast, anti-inflammatory effects were unaffected in CLX mice in which skin innervation at the ST36 site was selectively eliminated (Fig. 4d, e). Consistently, superficial intradermal 0.5-mA ES of the ST36 acupoint failed to produce anti-inflammatory effects (Extended Data Fig. 11a, b). Furthermore, no anti-inflammatory effects were evoked when 0.5-mA ES was conducted at the midline region of the posterior hindlegs, by inserting electric needles through the Chengjin (BL56) acupoint, with tips flanking the skin-innervating sural nerve[24] (Extended

Data Fig. 11c, d). Thus, the vagal–adrenal anti-inflammatory axis is probably mediated by PROKR2ADV sensory fibres that innervate deep limb fascia (Fig. 4f).

ES effects predicted by innervations

Last, we tested whether innervation patterns of PROKR2^{ADV} sensory fibres can retrospectively predict body regions at which low-intensity ES can or cannot drive anti-inflammatory effects. In contrast to prominent innervations of PROKR2^{ADV} sensory fibres in inner TA muscles (Extended Data Fig. 4d, e), PROKR2^{ADV} sensory fibres displayed sparse innervation in posterior muscles, including gastrocnemius muscles in the hindlegs and semitendinosus muscles at the thigh regions (Extended Data Fig. 11f, i). Consistently, 0.5-mA ES in these muscles failed to suppress TNF and IL-6 production (Extended Data Fig. 11e-j). Notably, the gastrocnemius and semitendinosus muscles do not contain traditional acupoints and have often been used as non-acupoint controls[10,25,26]. For a positive prediction, it should be noted that PROKR2^{ADV} neurons are also enriched in cervical C6–8 DRGs innervating the forelimbs (Extended Data Fig. 2a, b). We accordingly performed bilateral 0.5-mA ES of the Shousanli (LI10) acupoint, with the needle tips close to the deep branch of the radius nerve containing tdTomato^{+} fibres that innervate the radius periosteum (Extended Data Fig. 11k, l). This stimulation reduced TNF and IL-6 production that was dependent on PROKR2^{ADV} neurons and the vagal nerve (Extended Data Fig. 11m, n).

Discussion

Our studies provide a neuroanatomical explanation for the presence of acupoint selectivity (for example, the effective ST36 and LI10 acupoints versus the non-effective ST25 and BL56 acupoints) and acupoint specificity (for example, ST36 versus non-effective traditional non-acupoints in posterior hindlimb muscles) in driving a specific autonomic pathway: the vagal–adrenal axis (Fig. 4f). We argue that acupoint specificity, which has been long debated in the acupuncture field[27,28,29], is an operational definition that depends on the stimulation intensities, the depth at which the needle is placed and the outcomes measured. For example, for low-intensity ES, deep but not superficial stimulation of the ST36 site is crucial for driving the vagal–adrenal axis, which probably reflects the requirement of electric needle tips close to the major nerve bundles containing PROKR2^{ADV} fibres that innervate deep limb fascia (Fig 4f). By contrast, spinal sympathetic reflexes, which are independent of PROKR2^{ADV} neurons, can be evoked by high-intensity ES at both ST25 and ST36 acupoints. These findings could pave the way to optimization of bioelectronic stimulation parameters to drive distinct autonomic pathways for treating specific diseases, including severe cytokine release syndromes, the management of which remains a major medical challenge[30].

Methods

Mice

All animal experiments were performed according to protocols approved by the Institutional Animal Care and Use Committee at the Dana-Farber Cancer Institute and followed NIH

guidelines. Mice were kept in a temperature- and humidity-controlled room with a 12-h/12-h light/dark cycle and had ad libitum access to standard laboratory mouse pellet food and water. The *Prokr2*^{cre} transgenic mouse line was generated by the Gene Expression Nervous System Atlas (GENSAT) project[31] and acquired from MMRRC, University of California, Davis (MMRRC_034638-UCD). C57BL/6J male mice (000664), *Rosa26-loxP-stop-loxP-frt-stop-frt-tdTomato* mice (Ai65, 021875), *Rosa26-loxP-stop-loxP-tdTomato* reporter mice (Ai14, 007908) and *Rosa26-loxP-stop-loxP-frt-stop-frt-CatCh-eYFP* mice (RC::FL-CatCh, 025109) were acquired from the Jackson Laboratory. The *Advillin*^{Flpo} mice were acquired from the D. D. Ginty laboratory[14]. *Tau-loxP-stop-loxP-frt-stop-frt-DTR* mice were acquired from the M. Goulding group[32].

To generate PROKR2^{ADV}-neuron-ablated mice, 6–10-week-old *Prokr2*$^{cre/+}$;*Advillin*$^{Flpo/+}$;*Tau*$^{ds\text{-}DTR/+}$ mice (which also carry an Ai14 reporter allele) were intraperitoneally injected with DTX (20 μg kg–1, Sigma-Aldrich, D0564) for 5 consecutive days. LPS challenge and histochemical analyses were performed 4 weeks later. Littermates lacking either the *Advillin*^{Flpo} or the *Prokr2*^{cre} allele but receiving the same DTX injections were used as controls. Animals were randomly allocated into experimental groups, and investigators were blinded to the genotypes for survival analyses and for quantitative histochemical analyses. Males were used for this study (see the section ‘LPS experiments in mice’ for the reason), and sample sizes are described in the figure legends.

LPS experiments in mice

LPS from *Escherichia coli* 0111:B4 (L2630, Sigma-Aldrich) was formulated as a 10 mg ml–1 solution in sterile, pyrogen-free PBS (Gibco Life Technologies) and stored at 4 °C. Mice were intraperitoneally injected with a LD_{80} (80% lethality rate) dose of LPS (8 mg kg–1 for C57BL/6J male mice and 12 mg kg^{-1} for male mice with a mixed genetic background). Preliminary studies showed that females showed differential sensitivity to LPS, and the current studies focused on male mice. Blood was collected 1.5 h after LPS injection for the measurement of cytokines. Mouse survival rate was monitored as previously described11.

ES

Mice were anaesthetized with isoflurane (0.5–1.5%) and the body temperature was maintained using a heating pad. ES was conducted with pairs of unipolar stainless-steel acupuncture needles (0.16 × 7 mm). The electrical current range was set at 0, 0.5, 1.0 or 3.0 mA, and the stimulation lasted for 15 min, with a pulse width of 50 μs and a frequency of 10 Hz controlled using a stimulator (Model 3800, A-M Systems) and 4 isolators (Model 3820, A-M Systems). For ES at hindlimb ST36 (Zusanli) acupoints, two pairs of needles were inserted into the regions located about 4-mm down from the knee joint and about 2-mm lateral to the anterior tubercle of the tibia. For deep-tissue ES, the needles were perpendicularly inserted into the TA muscle, with a depth of 3–4 mm and the needle tips close to the deep and superficial peroneal nerves. Note that this focal electric stimulation mode, with the positive and negative electric needles separated by 1 mm, was different from the diffuse simulation mode used by Torress-Rosas et al.[10], in which the current entered the left leg and came out of the right leg. For shallow ES at the ST36 site, the electric needles were obliquely inserted 3–4 mm into the skin dermal tissue. For ES at the abdominal ST25

(Tianshu) acupoints, two pairs of electric needles were obliquely and bilaterally inserted 3–4-mm deep into the abdominal muscle layers. These two ST25 acupoints are located at the intersections defined by 5-mm lateral to, and the upper two-thirds and the lower one-third of, the line between the xiphoid process and the pubic symphysis upper border. To bilaterally stimulate the sural nerve, a pair of electrodes was obliquely inserted 3–4 mm through the skin and with the tips flanking the sural nerve. The insertion site was the Chengjin (BL56) acupoint, which is located at the posterior aspect of the lower leg, 4-mm below the popliteal fossa and in the centre of the belly. For bilateral ES within the lateral gastrocnemius muscles in the hind legs, two pairs of electric needles were perpendicularly inserted at a depth of 3–4 mm. This insertion site is located 4 mm below the popliteal fossa and 3 mm lateral to the smaller saphenous vein, with the needling spots in each leg aligned along the proximal-to-distal direction and parallel to the saphenous vein. This insertion site is far away from major nerve bundles within the hindlimb region. For bilateral ES within the semitendinosus muscles of the posterior thigh regions, two pairs of electric needles were perpendicularly inserted at a depth of 3–4 mm. The insertion sites were located 1 cm distal to the tail base and about 2.5 cm away from the knee joint. For bilateral ES at forelimb LI10 (Shousanli) acupoints, which are located at the dorsal radial side of the forelimb and about 0.5-cm down from the cubital crease, two pairs of needles were perpendicularly inserted and into the supinator muscle at a depth of 2–3 mm and the needle tips close to the deep branch of the radius nerve.

ES-evoked Fos induction in the DMV, spinal sympathetic preganglionic neurons and sympathetic ganglia, ES-evoked systemic catecholamine release, and ES-evoked effects on LPS-induced systemic inflammation and mortality were carried out as previously described[11].

Optical stimulation

Adult control and *Prokr2*^{Adv}-*CatCh* mice were anaesthetized with 0.5–1.5% isoflurane and a heating pad was used to maintain body temperature. A 21-gauge needle was used to puncture a 3-mm-deep hole in the ST36 (perpendicularly) acupoint, and an optic fibre was then implanted into the hole. The mice then received 15 min of 473-nm blue-light stimulation (10 Hz, 50-μs pulse width, 10 mW or 30 mW, Opto Engine, Laser Model PSU-III-LED). Optogenetic stimulation was controlled by the combination of custom programs written in Bonsai software (2.3.1) and Doric Neuroscience Studio (4.1.502) through an Arduino circuit board (Uno, Arduino), and custom sketches were written in Arduino software (1.8.7). The light output of each optical fibre was measured with a laser power meter (TS2, CNI), with laser intensities set at 10 mW or 30 mW.

For studying 473-nm blue-light-stimulation-evoked Fos induction in the spinal cord, the hindbrain and sympathetic ganglia, optic stimulation was performed for 15 min. Two hours later, the mice were perfused for tissue collection. For studying the impact of optical simulation on LPS-induced systemic inflammation and mortality, optic stimulation was performed for 15 min before LPS injection. For studying the systemic release of noradrenaline, adrenaline and dopamine, optic stimulation was performed for 15 min, and 15

min later, blood samples were collected. Both control littermates and *Prokr2*^{Adv}*-CatCh* mice received optic stimulation.

Neurectomy

Animals were anaesthetized with inhaled isoflurane (2–3%). Surgeries were performed 3 days before ES. The analgesic compound meloxicam (2 mg kg^{-1}, subcutaneous) was given every 24 h twice. Antibiotic (enrofloxacin, 2.5 mg kg^{-1}, subcutaneous; Baytril, Bayer Health Care) was given immediately after surgery and every 12 h until 24 h before the LPS challenge. Subdiaphragmatic vagotomy was performed as previously described[11]. For bilateral common peroneal neurectomy, lateral cutaneous neurectomy or tibial neurectomy, a thigh incision in each leg was performed to expose the common peroneal nerve, the lateral cutaneous sural nerve and the tibial nerve, and one of these nerves was stabilized with nylon thread and then sectioned. In control mice (sham surgery), the respective nerves were exposed and isolated from the surrounding tissue without transection.

Vagal efferent nerve recording

Mice were anaesthetized with 1–1.75% isoflurane in the supine position. Body temperature was maintained at 37.0 ± 0.5 °C with a servo-controlled temperature pad (TC-1000; CWE). A midline cervical incision was made, and the connective tissue overlying the vagus nerve was removed (using a microscope to perform the procedure). A segment (about 15 mm) of the left vagus nerve was isolated and the peripheral end crushed. The right vagus nerve was left intact. The vagus nerve was placed over a bipolar stainless silver wire hook electrode (AS632, Cooner Wire) that was positioned rostral to the crushed nerve end to measure multifibre vagal efferent nerve activity, without primary afferent inputs. The ground electrode was placed between the skin and right salivary gland. Electrodes and nerves were embedded in mineral oil (Kwik-Sil, WPI). Optic fibres were then bilaterally inserted into ST36 regions, as described above. Physiological signals were band-pass-filtered between 100 Hz and 30 kHz, and received a 50-fold gain with an amplifier (BMA-400 amplifier, CWE). All signals were referenced to the ground. The analog signals were digitized (Micro3 1401, CED) and processed using Spike 2 software (v.8.08, CED). Following acquisition of baseline activity (20–30 min), the mice were treated with 473-nm blue-light stimulation for 2 min (10 Hz, 50-μs pulse width, 10 mW, Opto Engine, Laser Model PSU-III-LED). Raw signals were filtered using a high-pass filter at 160 Hz followed by a smoothing algorithm consisting of a finite impulse response filter. Waveform analysis was done on the filtered recordings using a user-defined adaptive threshold method and wave-mark parameters (spike shape with a total spike time of approximately 3 ms). Identified waveforms were manually categorized as neural spikes or other (for example, cardiac or respiratory) signals. The signals corresponding to cardiac and respiratory components were manually removed. Neural spikes, defined by compound action potentials with amplitudes 1.5-fold larger than baseline potentials, were identified to calculate the firing rate.

Histology of tissue sections

Animals were euthanized with CO2 and then transcardially perfused with 4% paraformaldehyde (PFA). The DRG, spinal cord, brain and sympathetic ganglia were dissected and then post-fixed in the same fixatives overnight at 4 °C. The skin, abdominal

wall, adrenal glands, colon and hindlimbs were dissected and post-fixed in Zamboni's solution overnight at 4 °C. Fixed hindlimbs were rinsed with PBS and decalcified in 10% EDTA at 4 °C for at least 2 weeks. These tissues were cryopreserved in 30% sucrose in PBS overnight and then embedded in Tissue-Tek OCT compound (Sakura Finetek). Subsequent immunohistochemistry on 30-μm-thick sections through collected tissues was performed as previously described11 with the following antibodies: rabbit anti-TUBB3 (1:1,000, ab52623, Abcam); rabbit anti-Fos (1:500, ABE457, Millipore); goat anti-ChAT (1:500, AB144P, Millipore); rabbit anti-GFP (1:500, A11122, Invitrogen); chicken anti-GFP (1:500, A10262, Invitrogen); rat anti-TRKA (1:200, AF1056, R&D); chicken anti-NEFH (1:500, NFH, Aves Labs); rabbit anti-CGRP (1:1,000, PC205, Millipore); rabbit anti-PV (1:1,000, PV 27, Swant); Alexa Fluor 488-conjugated IB4 (1:500, I21411, Invitrogen); and Alexa Fluor 405-, 488- or 594-conjugated donkey anti-goat, rabbit, rat, chicken IgG (1:500; 711-545-152, 705-585-003, 705-545-003, 705-475-147, 711-585-152 and 712-476-150; Jackson ImmunoResearch). Images were acquired using a laser-scanning confocal microscope (Zeiss LSM700) or a Zeiss Axio Observer.Z1 epifluorescence microscope system.

In situ hybridization (ISH) combined with immunohistochemistry procedures were performed as previously described[33]. Both fluorescence and ISH signals were collected using a fluorescence microscope. The tdTomato and immunohistochemical fluorescence signals were photographed from the slices followed by ISH. The pseudo-fluorescent ISH signals were converted from bright-field images and then merged onto the tdTomato images using Photoshop (CS6, Adobe).

To characterize and quantify PROKR2^{ADV}-tdTomato^{+} DRG neurons and other DRG neurons retrogradely labelled with Fluoro-gold from the ST36 and ST25 regions, we analysed 4–8 sections each of collected L4–L5 and T8–T10 DRGs. Adult male mice (n = 4–5) were used. To examine neurons activated by ES or 473-nm blue-light stimulation at ST36 regions, we quantified Fos+ cells in transverse sections through sympathetic ganglia, parasagittal sections through the intermediate lateral nuclei of the spinal cord or coronal hindbrain sections through the DMV. A total of 5–10 sections was analysed using ImageJ (2.0.0-rc-69/1.52p) for each sample, with 3–5 adult male mice per group. To test ablation efficiency, we used 5 pairs of adult control and ablated mice and, for each mouse, analysed 4–8 sections through lumbar DRGs, spinal cord and brain regions.

Whole-mount immunohistochemistry

The peritoneum was dissected from the abdominal ST25 region from *Prokr2^{ADV}-tdTomato* mice without perfusion, cut into 1 × 1-cm pieces and fixed with Zamboni's solution overnight at 4 °C. The tissue was then rinsed in PBS and washed 3 times with PBS containing 1% Triton X-100 and 1% Tween-20 (1% PBST) for 1 h each. The peritoneum samples were then incubated with the following primary antibodies in 1% PBST containing 5% donkey serum and 20% dimethylsulfoxide at room temperature for 2 days: rabbit anti-TUBB3 (1:200, ab52623, Abcam) or goat anti-mCherry (1:500, AB0040-200, Acris). Tissues were then washed three times with 1% PBST for 1 h each, and then transferred to the following secondary antibodies in 1% PBST containing 5% donkey serum and 20%

dimethylsulfoxide and incubated at room temperature overnight: Alexa Fluor 488, 594 donkey anti-rabbit, goat IgG (1:500; 711-545-152, 705-585-003; Jackson ImmunoResearch). Tissues were washed three times with 1% PBST for 1 h each. The peritoneum was then dehydrated in 50% methanol for 5 min and 100% methanol for 20 min, 3 times, and cleared in benzyl alcohol (Sigma, 402834) and benzyl benzoate (Sigma B-6630; 1:2) at room temperature for 20 min.

The interosseous membranes were dissected from the hindlimbs of *Prokr2*^{ADV}*-tdTomato* mice following transcardial perfusion with 4% PFA, and post-fixed with Zamboni's solution overnight at 4 °C. The membranes were then washed 3 times with 1% PBS and incubated overnight at room temperature in the same buffer containing the following primary antibodies: rabbit anti-S100 (1:300, Sigma, SAB4502708) and chicken anti-NEFH (1:300, NFH, Aves Labs). After washing three times with 1% PBST for 1 h each, the membrane was stained with the following secondary antibodies overnight at room temperature: Alexa Fluor 488, 405 donkey anti-chicken, rabbit lgG (1:500; 703-545-155, 711-475-152; Jackson ImmunoResearch). On the third day, tissues were washed with 1% PBST for 3 times for 1 h each and mounted onto gelatin-coated slides and coverslipped with Fluoromount. Images were acquired using a laser-scanning confocal microscope (Zeiss LSM700).

Cytokine and catecholamine measurement

The serum concentrations of TNF, IL-6 and catecholamines (adrenaline, noradrenaline and dopamine) were analysed using ELISA kits as previously described[11].

Cell culture and DRG preparation

DRGs were isolated from adult *Prokr2*^{Adv}*-CatCh* mice and their control littermates and kept in sterile ice-cold 1× HBSS medium (Invitrogen) throughout the dissection. After removal of connective tissues, DRGs were transferred to 1 ml Ca^{2+}/Mg^{2+}-free HBSS containing 2 μl saturated NaHCO3, 0.35 mg l-cysteine and 20 U papain (Worthington), and then incubated at 37 °C and 5% CO2 for 10 min. DRGs were spun down and the supernatant was removed. Ca^{2+}/Mg^{2+}-free HBSS (1 ml) containing 4 mg collagenase type II and 1.25 mg dispase type II (all from Sigma-Aldrich) was added and the samples were incubated at 37 °C and 5% CO2 for another 20 min. DRGs were then washed twice with 10 ml neurobasal medium containing 2% B-27 supplement, 1% l-glutamine, 100 U ml–1 penicillin plus 100 μg ml–1 streptomycin, and mechanically triturated using fire-polished Pasteur pipettes 3–5 times. After trituration, ganglia were briefly centrifuged (1,000 r.p.m. maximum) and resuspended with the above medium containing 50 ng ml–1 nerve growth factor. The dissociated neurons were plated on a 12 × 12-mm coverslip previously coated with laminin (BD Bioscience) and poly-d-lysine (Sigma-Aldrich). Cells were incubated for 16–24 h at 37 °C and 5% CO2 before electrophysiological recordings were performed.

Whole-cell electrophysiology

Whole-cell recordings were performed using an Axon 700B amplifier (Molecular Devices) at room temperature (22–24 °C) on the stage of an upright microscope (Olympus, BX51WI, Japan) equipped with ×5 and ×60 water-immersion objectives and infrared differential interference contrast (IR-DIC). Pipettes pulled from borosilicate glass (BF 150-86-10; Sutter

Instrument) with a Sutter P-1000 pipette puller had resistance values of 3–6 MΩ for whole-cell recordings when filled with pipette solution containing the following (in mM): 130 potassium gluconate, 5 KCl, 4 Na2ATP, 0.5 NaGTP, 20 HEPES and 0.5 EGTA. Bath solution, pH 7.4, contained the following (in mM): 150 NaCl, 5 KCl, 1 CaCl2, 1 MgCl2, 10 HEPES and 10 glucose. Multimode optic fibres coupled to diode-pumped solid-state lasers of specific wavelengths (473-nm blue laser, Opto Engine, Laser Model PSU-III-LED) were used for optical stimulation of DRG neurons. Light intensities were measured using a TS2 power meter coupled to a LP100 photodiode sensor (CNI). The 473-nm blue light (10 Hz, 50-μs wave width, 10 mW) was delivered, and the responses were recorded in the voltage clamp mode (holding membrane potential at −60 mV) and then in the current clamp mode. Data were acquired using Clampex 10.4 software (Molecular Devices). Currents were filtered at 2 kHz and digitized at 10 kHz. Data were analysed and plotted using Clampfit 10 (Molecular Devices).

Fluoro-gold retrograde labelling

For retrograde labelling from the deep tissues at ST36 regions, adult *Prokr2*^{Adv}*-tdTomato* mice were anaesthetized with inhaled isoflurane. Hair was shaved and an incision was made at the ST36 region. Fluoro-gold (4 μl; Fluorochrome, 2% in water) was injected into the TA muscle at 2–3-mm depth using a Hamilton microsyringe (30-gauge needle). Injection sites were swabbed to remove any excess of tracer, and the skin was closed using Vicryl sutures. Animals were allowed to recover for 5 days before dissection of lumbar DRGs. Co-staining with IB4 binding was done on DRG sections to check for potential leakage of Fluoro-gold into the skin. IB4 is a marker for sensory neurons innervating the skin epidermis. Only those DRGs with less than 5% of labelled neurons overlapping with IB4 were used for further analysis. For retrograde labelling from the skin epidermis and hair follicles, adult *Prokr2*^{Adv}*-tdTomato* mice were anaesthetized with inhaled isoflurane. Hair was shaved at the ST36 region (for labelling L4–L5 DRGs) and at the ST25 region (for labelling T8–T10 DRGs), and we used labelling tape and sandpaper to remove the skin stratum corneum, followed by topical application of 4 μl Fluoro-gold. Animals were allowed to recover for 5 days before dissection of lumbar and thoracic DRGs. Quantitative analyses were done on lumbar L4–L5 DRGs and T8–T10 DRGs from at least 4 mice.

For labelling spinal neurons projecting to the NTS in the hindbrain, mice were anaesthetized with an intraperitoneal injection of ketamine/xylazine (87.5/12.5 mg kg–1) mixture. After anaesthesia, the mouse was placed prone on a stereotaxic apparatus (Stoelting), and body temperature was maintained at 37 °C using a heating pad. Occipital craniotomy was performed to expose the dorsal surface over the NTS. A glass micropipette, pulled from borosilicate glass (BF 150-86-10, Sutter Instrument) with a Sutter P-1000 pipette puller, was used for microinjecting Fluoro-gold into the dorsal and intermediate NTS at the level of calamus scriptorius (approximate stereotaxic coordinates: two bilateral rostral sites: medial–lateral: ±0.3 mm, anterior–posterior: 0.2 mm, dorsal–ventral: −0.2 mm; two bilateral caudal sites: medial–lateral: ±0.4 mm, anterior–posterior: 0.3 mm, dorsal–ventral: −0.3 mm), using a syringe pump (Harvard Apparatus). In total, 400 nl Fluoro-gold (Fluorochrome, 2% in water, 100 nl per injection) was injected into the NTS. After surgery, the analgesic compound meloxicam (2 mg kg^{-1}, subcutaneous) was given every 24 h twice. Mice were

then given a 5-day recovery period before optical stimulation or ES at hindlimb ST36 regions. Quantitative histochemical analyses were performed for three animals.

For labelling vagal efferent neurons projecting to the adrenal medulla, adult control littermates and *Prokr2*^{Adv}*-CatCh* mice were anaesthetized with isoflurane (2–3%), and the left and right adrenal glands were exposed through a flank incision. Fluoro-gold (2 μl; Fluorochrome, 2% in water) was injected into the adrenal medulla using a glass micropipette attached to a 10-μl Hamilton syringe. The abdominal wall and skin were closed using Vicryl sutures. The analgesic compound meloxicam (2 mg kg^{-1}, subcutaneous) was given every 24 h twice. Mice were then given a 5-day recovery period before optical stimulation at hindlimb ST36 regions. Quantitative analyses were done performed for three animals.

Statistics

Results are expressed as mean ± s.e.m. Statistical analyses were done using GraphPad Prism 7 and SigmaStat 3.5 software. All datasets were tested for normality for t-tests, and if normality failed, the Mann–Whitney rank-sum test was used. Survival rates are expressed using Kaplan–Meier curves, and comparisons of survival curves were performed with a Mantel–Cox log-rank test. For pairwise comparisons (two samples involved), data were analysed with two-sided Student's unpaired t-test. For the comparison of PROKR2^{ADV}-tdTomato^{+} fibres innervating different muscles, data were analysed using one-way analysis of variance (ANOVA) followed by post hoc Tukey's test. Other data with multiple variables (such as different ES modes on mice with different genotypes) were analysed using two-way ANOVA followed by post hoc Tukey's tests. No statistical methods were used to predetermine sample sizes. Sample sizes for all histochemical, cytokine and transmitter measurements were chosen according to recently reported studies[10,11]. For survival rate analyses, they normally required large sample sizes, with the power set at 0.8 and the confidence interval set at 95%; we realistically aimed to detect major changes, such as a change of survival rates from 20% to 60–80% or vice versa, which required n = 20–25 per group. Differences were considered significant when $P < 0.05$.

Extended Data

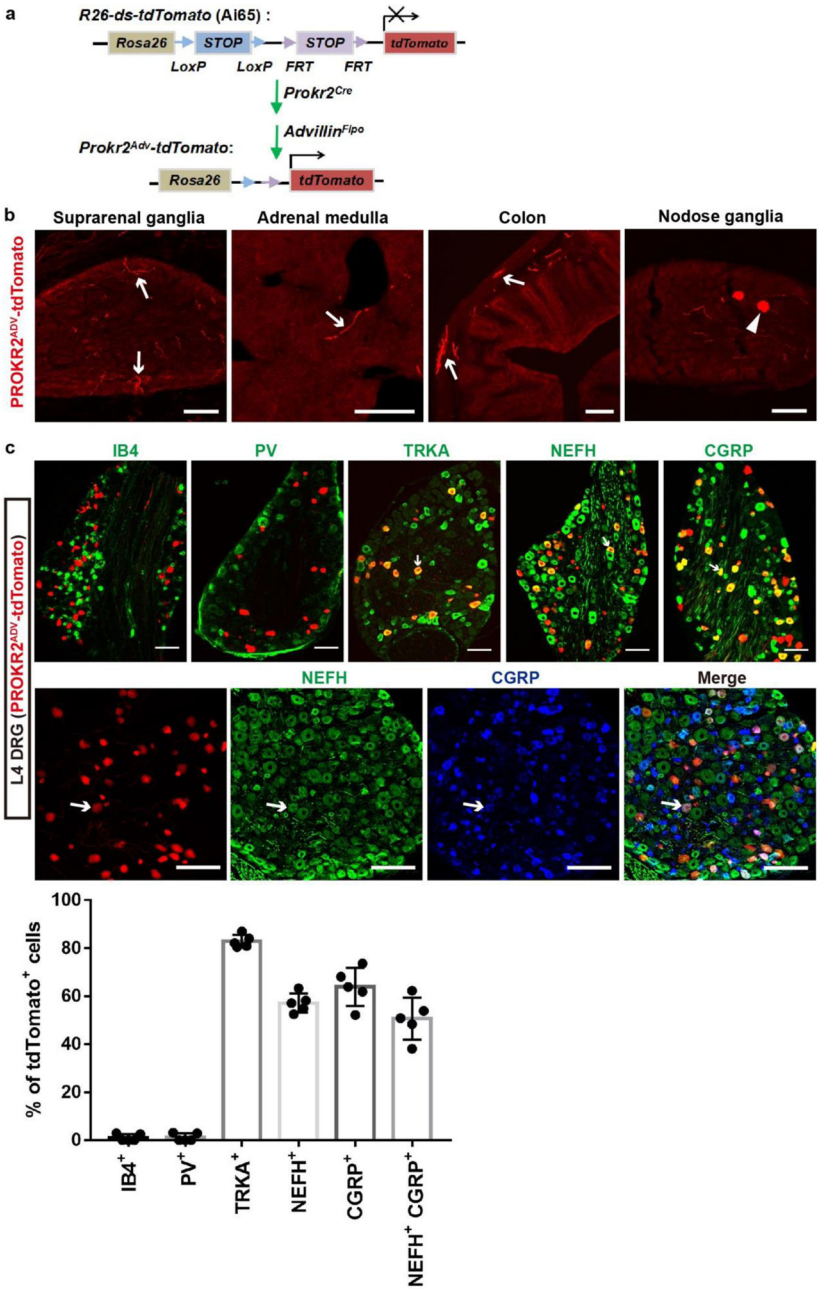

Extended Data Fig. 1. Intersectional marking and characterization of PROKR2^{ADV} neurons.

a, Schematic description of the intersectional genetic strategy for generating *Prokr2^{Adv}-tdTomato* mice, in which tdTomato expression was confined to PROKR2^{ADV} sensory neurons upon removal of two *STOP* cassettes from the *ROSA26* allele by the Cre and Flpo recombinases. *Advillin^{Flpo}* drove Flpo expression restricted to sensory neurons, such that DRG neurons with developmental coexpression of PROKR2-Cre and ADVILLIN-Flpo were marked by tdTomato. **b,** Representative sections through suprarenal sympathetic ganglia, adrenal medulla where chromaffin cells were located, the colon that should contain

enteric ganglia, and nodose ganglia from *Prokr2*^{Adv}*-tdTomato* mice. The intersectional genetic strategy only labeled one or two cells per section in nodose ganglia. Arrows indicate tdTomato^{+} fibers, but not somas, likely from DRG neurons or from those rare nodose sensory neurons. In other words, PROKR2^{ADV}-tdTomato did not label any autonomic neurons and adrenal chromaffin cells. n = 5 mice per group. **c**, L4-5 DRG sections from adult *Prokr2*^{Adv}*-tdTomato* mice. Top panels show double immunostaining of tdTomato (red) with markers for nonperptidergic neurons (IB4: isolectin B4), proprioceptors (PV: parvalbumin), TRKA-lineage neurons (TRKA), myelinated neurons (NEFH: the neurofilament heavy chain protein), and peptidergic neurons (CGRP: the calcitonin gene-related peptide). Bottom panels show triple staining of tdTomato with NEFH and CGRP. Arrows indicate co-localization. n = 5 mice for each marker. Data are shown as mean ± SEM. Scale bars, 100 μm.

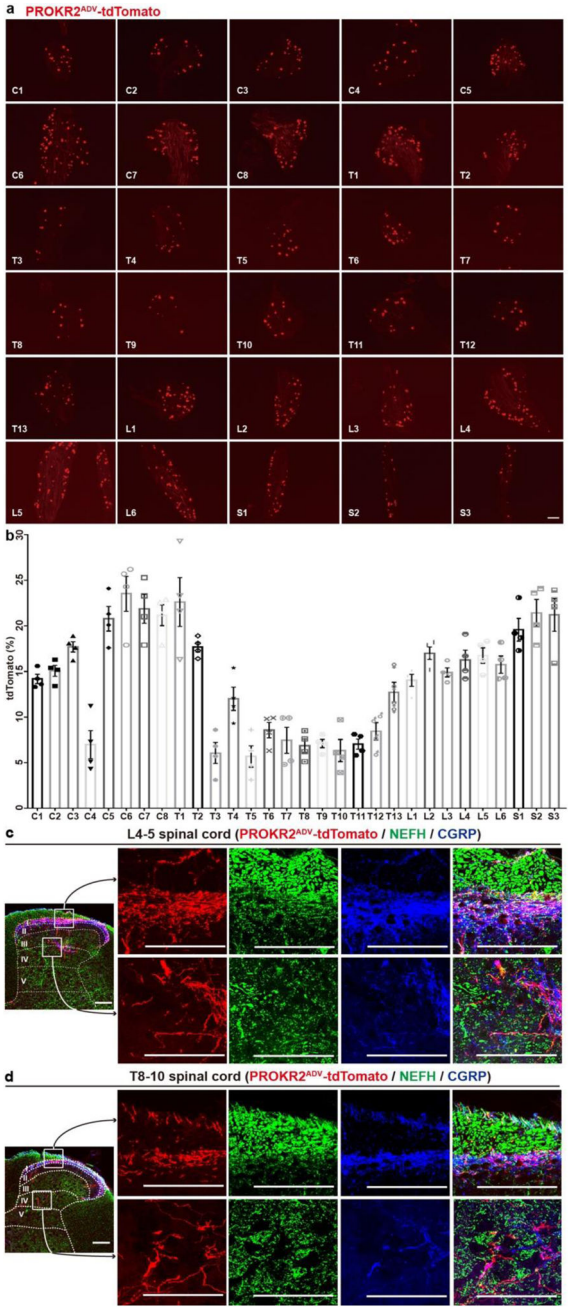

Extended Data Fig. 2. Percentages of PROKR2^{ADV}-tdTomato^{+} neurons in DRGs and their innervation in the spinal cord.

a, Representative sections through cervical (C1-C8), thoracic (T1-T13), lumbar (L1-L6), and sacral (S1-S3) DRGs from the adult *Prokr2^{Adv}-tdTomato* mice. **b,** Percentages of DRG neurons [determined by the expression of TUBB3 (not shown), a pan-neuronal marker] expressing tdTomato along the anterior-posterior axis; n = 4 mice. Note higher representations at the limb levels (e.g., C6-C8 and L3-L6 DRGs that innervate the forelimbs and hindlimbs, respectively) compared with thoracic DRGs. **c, d,** Sections through L4-5 lumbar and T8-10 thoracic levels of the spinal cord from *Prokr2^{Adv}-tdTomato* mice were triple stained [tdTomato (red), the NEFH protein (green) and CGRP(blue)]. tdTomato^{+}

terminals were predominantly located in superficial laminae (**c,d**, top boxed panels), but also seen in deep laminae (III-V) (**c,d**, bottom boxed panels). Qualitatively, tdTomato^{+} fibers in the superficial laminae appeared to show more co-staining with CGRP and NEFH, in comparison with those in deep laminae. n = 5 mice per group. Data are shown as mean ± SEM. Scale bars, 100 μm.

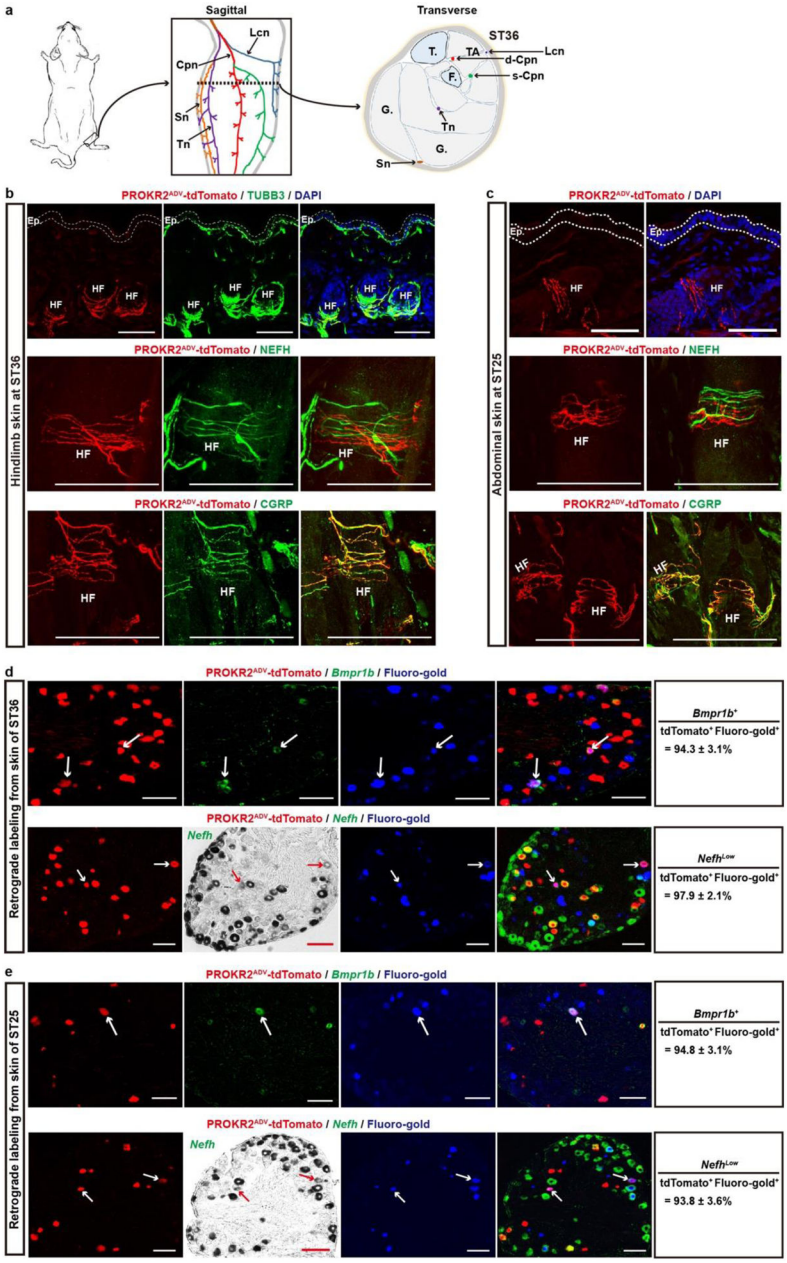

Extended Data Fig. 3. Skin innervation by PROKR2^{ADV} neurons in the hindlimb ST36 and abdominal ST25 acupoint regions.

a, Left, schematics showing the ST36 location. Middle: schematic showing of several but not all nerve bundles in the hindleg. Right: a schematic transverse section through the hindlimb ST36 region. TA: the tibialis anterior muscle. “T.”: tibia. “F.”: fibula. G.:

gastrocnemius. Cpn: the common peroneal nerve and its deep (d-Cpn) and superficial (s-Cpn) branches. Lcn: the lateral cutaneous nerve. Tn: the tibial nerve. Sn: the sural nerve. **b,** Representative sections through the skin of the ST36 region of *Prokr2*^{Adv}*-tdTomato* mice. tdTomato^{+} fibers formed circumferential endings surrounding hair follicles ("HF"), without innervation to the epidermis ("Ep."), in contrast with epidermal presence of TUBB3^{+} nerve fibers (green). DAPI (blue) staining showed cell nuclei. Note that these circumferential endings coexpressed CGRP but lacked detectable expression of the NEFH protein. n = 5 mice. **c,** Representative skin sections through the abdominal ST25 region in *Prokr2*^{Adv}*-tdTomato* mice. Top: tdTomato^{+} fibers (red) did not innervate the epidermis ("Ep."), with DAPI (blue) staining cell nuclei. Middle and bottom: NEFH-negative but CGRP-positive tdTomato^{+} fibers formed circumferential endings surrounding hair follicles ("HF"). n = 5 mice. **d, e,** Representative sections through L4-5 lumbar DRGs (d) or through T8-10 thoracic DRGs (e) from *Prokr2*^{Adv}*-tdTomato* mice, in which DRG neurons innervating the cutaneous tissue of ST36 and ST25 were retrogradely labeled with Fluoro-gold (blue). Note that most retrogradely labeled-PROKR2^{ADV}-tdTomato^{+} neurons in both sets of DRGs coexpressed *Bmpr1b* mRNA (arrows) and low levels of *Nefh* mRNA (arrows). n = 4 mice. The bright-field images of *Nefh* mRNA, which were easier for identification of cells with low versus high levels, were converted to become pseudo green color in merged images. Data are shown as mean ± SEM. Scale bars, 100 μm.

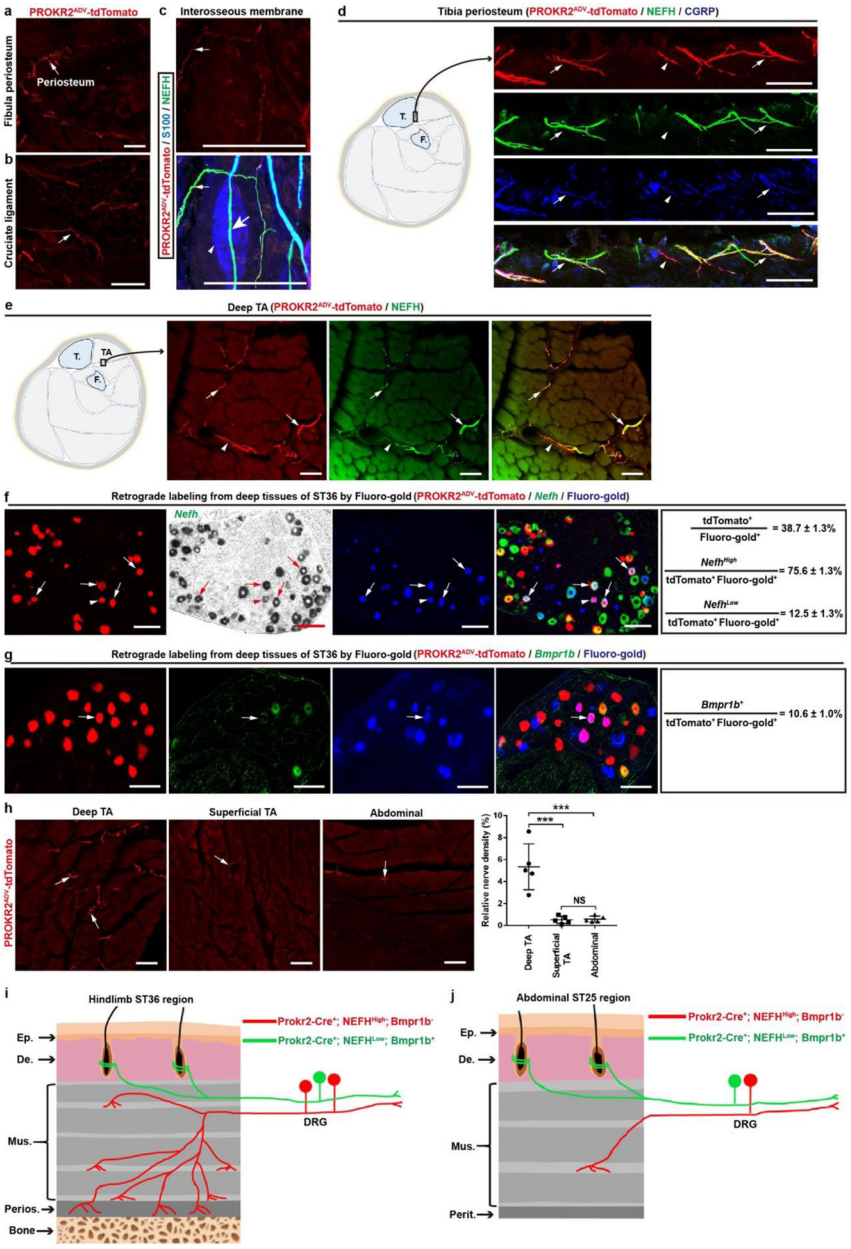

Extended Data Fig. 4. Innervation patterns by PROKR2^{ADV} neurons in deep fascial tissues at the hindlimb ST36 and abdominal ST25 regions.

a-c, tdTomato^{+} fibers innervated fibula periosteum (**a,** arrow) and the cruciate ligament (**b,** arrow), and tdTomato^{+};NEFH^{+} free nerve endings in the interosseous membrane located between bones (**c**, small arrow). tdTomato signals were, however, not detected in NEFH^{+} fibers (**c**, green, large arrow) passing through the S100^{+} Pacinian corpuscles (**c**, blue, arrowhead). n = 5 (**a**, **b**) or 2 (**c**) mice. **d,** Representative sections showing PROKR2^{ADV}-tdTomato^{+} fibers that innervated tibia periosteum of the ST36 region, 63.5 ± 4.1% of which were NEFH^{+} and CGRP^{+}. n = 5 mice. **e,** Representative transverse sections through the inner compartment of the tibialis anterior muscle (“TA”) at the ST36 region of *Prokr2^{Adv}-tdTomato* mice. Most tdTomato^{+} fibers coexpressed NEFH. n = 5

mice. **f, g,** Representative sections through L4-L5 lumbar DRGs from *Prokr2*^{Adv}*-tdTomato* mice, in which DRG neurons innervating deep ST36 tissues (deep muscles and possibly bones as well) were retrogradely labeled with Fluoro-gold (blue). Subsets of retrogradely labeled-PROKR2^{ADV}-tdTomato^{+} DRG neurons expressed *Nefh*^{High} (**f**, arrows), *Nefh*^{Low} (**f**, arrowhead), or *Bmpr1b* (**g**, arrow). n = 4 mice. **h,** Representative sections showing higher innervation densities of PROKR2^{ADV}-tdTomato^{+} fibers (arrows) in inner TA, compared with outer TA and abdominal muscles (one-way ANOVA, n = 5 mice per group; $F_{2, 12}$ = 25.098, $P < 0.001$; *post hoc* Tukey's test: ***$P < 0.001$; NS = not significant, $P = 0.995$). **i, j,** Schematics showing two major subtypes of PROKR2^{ADV} DRG neurons innervating hindlimb ST36 (**i**) and abdominal ST25 regions (**j**). *Nefh*^{High}; *Bmpr1b*$^{-}$ neurons densely innervate deep fascial tissues, including bone periosteum ("Perios.") plus the space between muscle bundles within the inner TA compartment, but show sparse innervation in the outer TA compartment at the ST36 region and at the abdominal muscle layers of the ST25 region. The *Nefh*^{Low}; *Bmpr1b*$^{+}$ neurons mainly form circumferential endings around hair follicles at both ST36 and ST25 regions, with few retrogradely labeled from deep fascia (not shown). Thoracic and lumbar DRGs also contain *Nefh*-negative neurons (~40%), and their target tissues remain to be determined since only a small subset (12.3%) of neurons retrogradely labeled from deep ST36 tissues were *Nefh*-negative. T.: tibia; F.: fibula; Ep.: epidermal; De.: dermis; Mus.: muscle; Perit.: peritoneum. Data are shown as mean ± SEM. Scale bars, 100 μm.

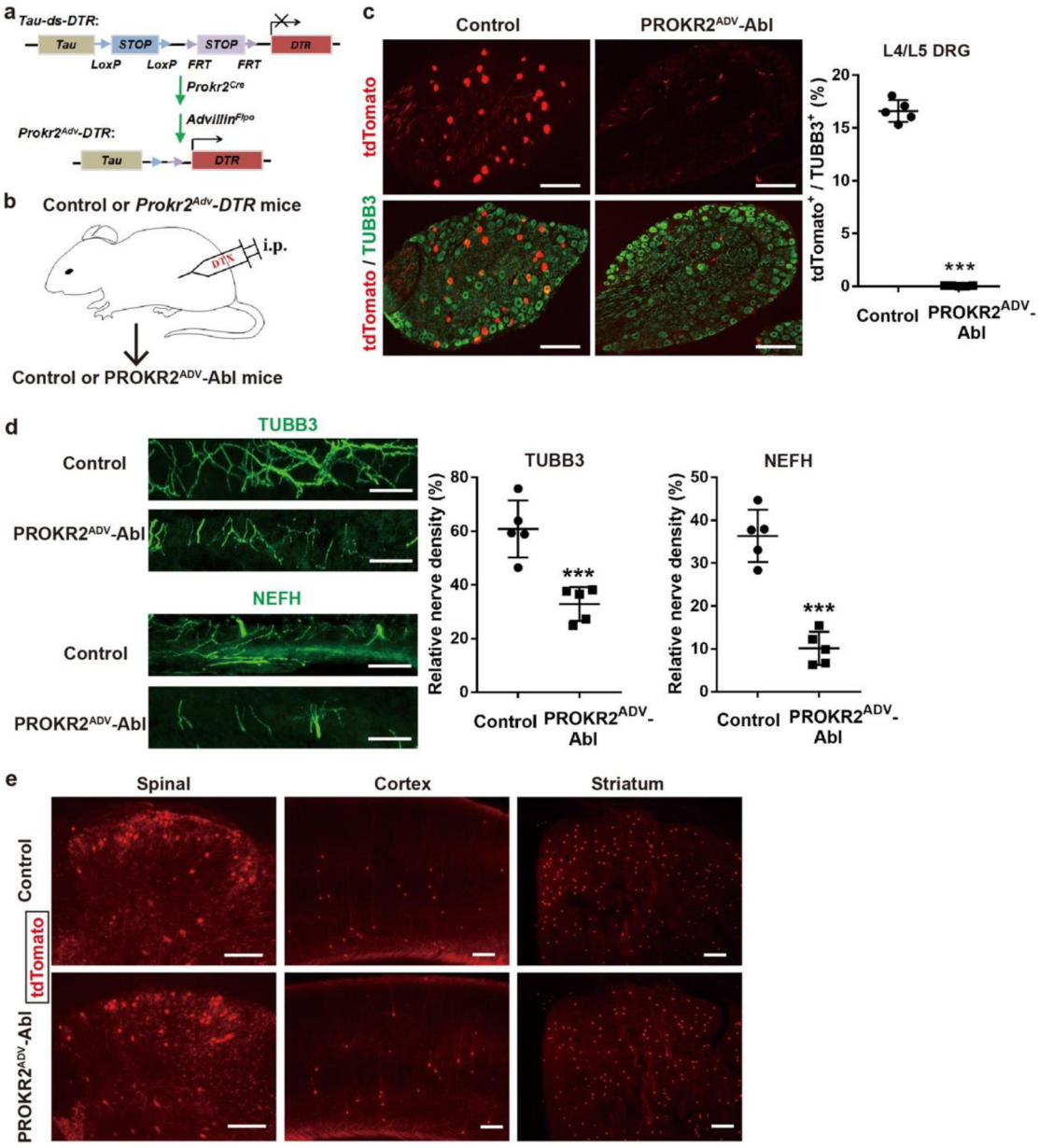

Extended Data Fig. 5. Intersectional genetic ablation of PROKR2^{ADV} DRG neurons.

a, Schematics of the intersectional genetic strategy for selectively driving the diphtheria toxin receptor ("DTR") in PROKR2^{Cre}-marked DRG neurons that coexpressed ADVILLIN-Flpo. This was achieved upon removal of two *STOP* cassettes from the intersectional allele of *Tau*, a pan-neural gene. A Cre-dependent *tdTomato* allele driven from the *ROSA26* promoter was included (not shown) to label all PROKR2-Cre^{+} cells with tdTomato, within or outside DRGs. **b,** Intraperitoneal injection ("i.p.") of the diphtheria toxin ("DTX") in *Prokr2^{Adv}-DTR* mice to create PROKR2^{ADV}-Abl mice, with littermates receive the same DTX injections as control. **c,** Ablation of PROKR2^{Cre}-tdTomato^{+} neurons in lumbar DRGs, as indicated by marked reduction in the percentage of TUBB3^{+} DRG neurons coexpressing tdTomato. n = 5 mice per group. Two-side student's unpaired *t*-test, $t_8 = 35.61$, ***$P <$

0.001. **d,** Representative images through tibia periosteum, showing reduction of TUBB3^{+} and NEFH^{+} fibers in PROKR2^{ADV}-Abl mice compared with control mice (n = 5 mice per group; two-side student's unpaired *t*-test; for TUBB3: $t_8 = 5.065$, ***$P = 0.001$; for NEFH: $t_8 = 8.122$, ***$P < 0.001$). **e,** Representative images showing the preservation of PROKR2^{Cre}-tdTomato^{+} neurons in the spinal cord as well as various brain regions such as the cortex and the striatum. n = 5 mice per group. Data are shown as mean ± SEM. Scale bars, 100 μm.

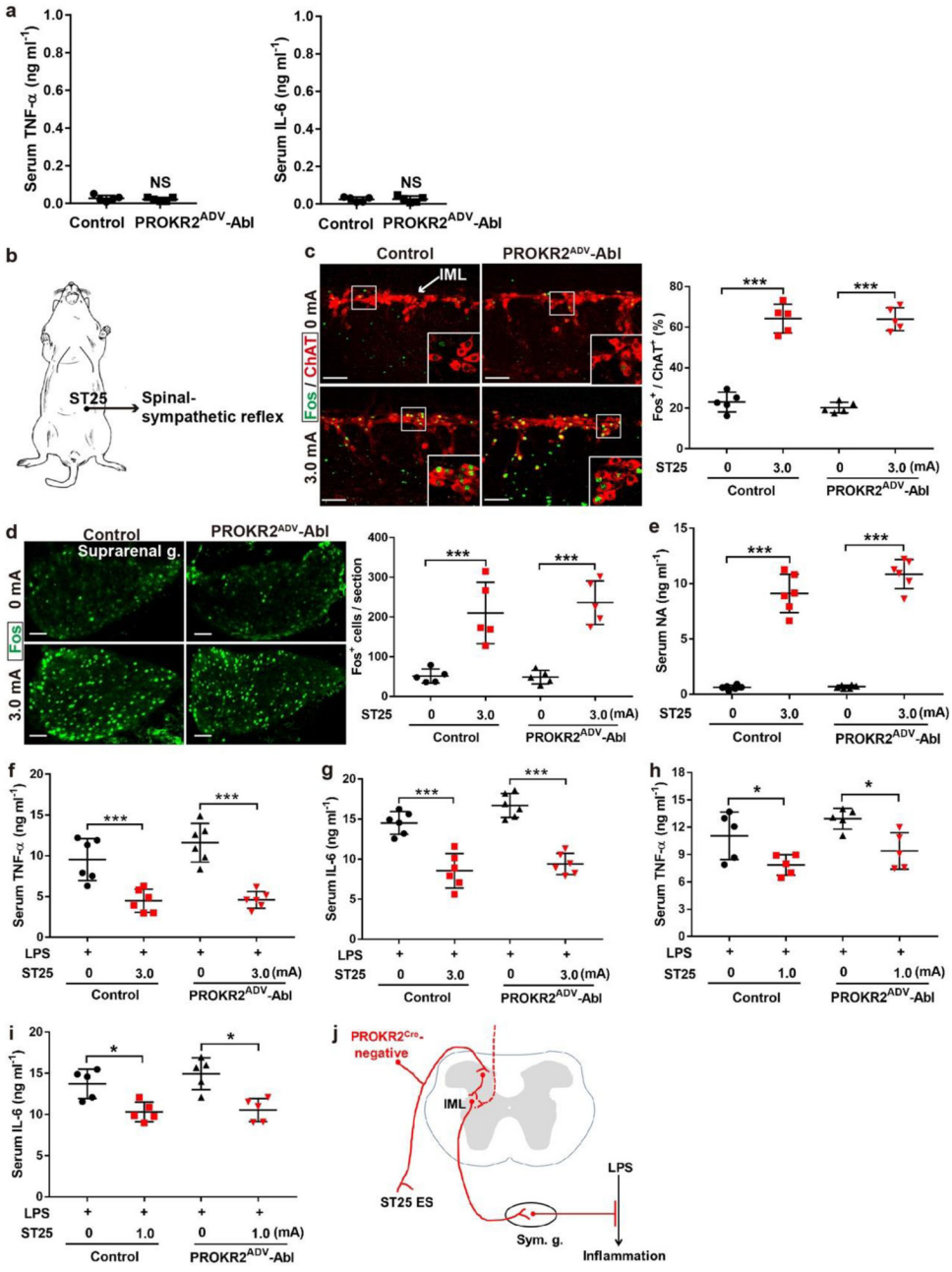

Extended Data Fig. 6. PROKR2^{ADV} neurons were dispensable for high-intensity ES of ST25 to drive sympathetic reflex and to produce anti-inflammatory effects.

a, Without LPS challenge, both control and PROKR2^{ADV}-Abl mice showed virtually non-detectable, indistinguishable levels of TNF-a and IL-6 in serum (two-side student's unpaired *t*-test, n = 5 mice per group; for TNF-a: $t_8 = 0.580$; NS, not significant, $P = 0.578$; for IL-6: $t_8 = 0.151$; NS, $P = 0.884$). **b,** Schematic description of 3.0 mA ES of the abdominal ST25 acupoint that drove spinal-sympathetic reflexes. **c,** No changes in 3.0 mA ST25 ES-evoked Fos (green) induction in ChAT^{+} preganglionic sympathetic efferent neurons in the spinal intermediolateral nuclei ("IML") between control and PROKR2^{ADV}-Abl mice (Two-way ANOVA, n = 5 mice per group, $F_{1, 16} = 0.421$, $P = 0.562$; *post-hoc* Tukey's test: ***$P < 0.001$). **d,** No changes in 3.0 mA ST25 ES-evoked Fos induction in the suprarenal sympathetic ganglia ("g.") (Two-way ANOVA, n = 5 mice per group, $F_{1, 16} = 0.290$, $P = 0.598$; *post-hoc* Tukey's test: ***$P < 0.001$). **e,** No changes in 3.0 mA ST25 ES-induced noradrenaline ("NA") release (two-way ANOVA, n = 6 per group, $F_{1, 20} = 4.093$, $P = 0.057$; *post hoc* Tukey test: ***$P < 0.001$). **f, g,** No changes in 3.0 mA ST25 ES-evoked reduction of LPS-induced TNF-a and IL-6 production (two-way ANOVA, n = 6 mice per group; for TNF-a: $F_{1, 20} = 1.851$, $P = 0.189$; *post-hoc* Tukey test: ***$P < 0.001$; for IL-6: $F_{1, 20} = 5.214$, $P = 0.133$; *post-hoc* Tukey test: ***$P < 0.001$). **h, i,** No marked changes in 1.0 mA ST25 ES-evoked reduction of LPS-induced TNF-a and IL-6 production (two-way ANOVA, n = 5 mice per group; for TNF-a: $F_{1, 16} = 4.357$, $P = 0.053$; *post-hoc* Tukey test: left *$P = 0.014$, right *$P = 0.018$; for IL-6: $F_{1, 16} = 1.019$, $P = 0.328$; *post-hoc* Tukey test: left *$P = 0.013$, right *$P = 0.015$). **j,** Schematics showing that PROKR2^{Cre}-negative sensory neurons preserved in PROKR2^{ADV}-Abl mice were sufficient to drive the spinal-sympathetic anti-inflammatory pathways in response to 1.0-3.0 mA ES of the abdominal ST25 acupoint. Sym. g.: sympathetic ganglia. Data are shown as mean ± SEM. Scale bars: 100 μm.

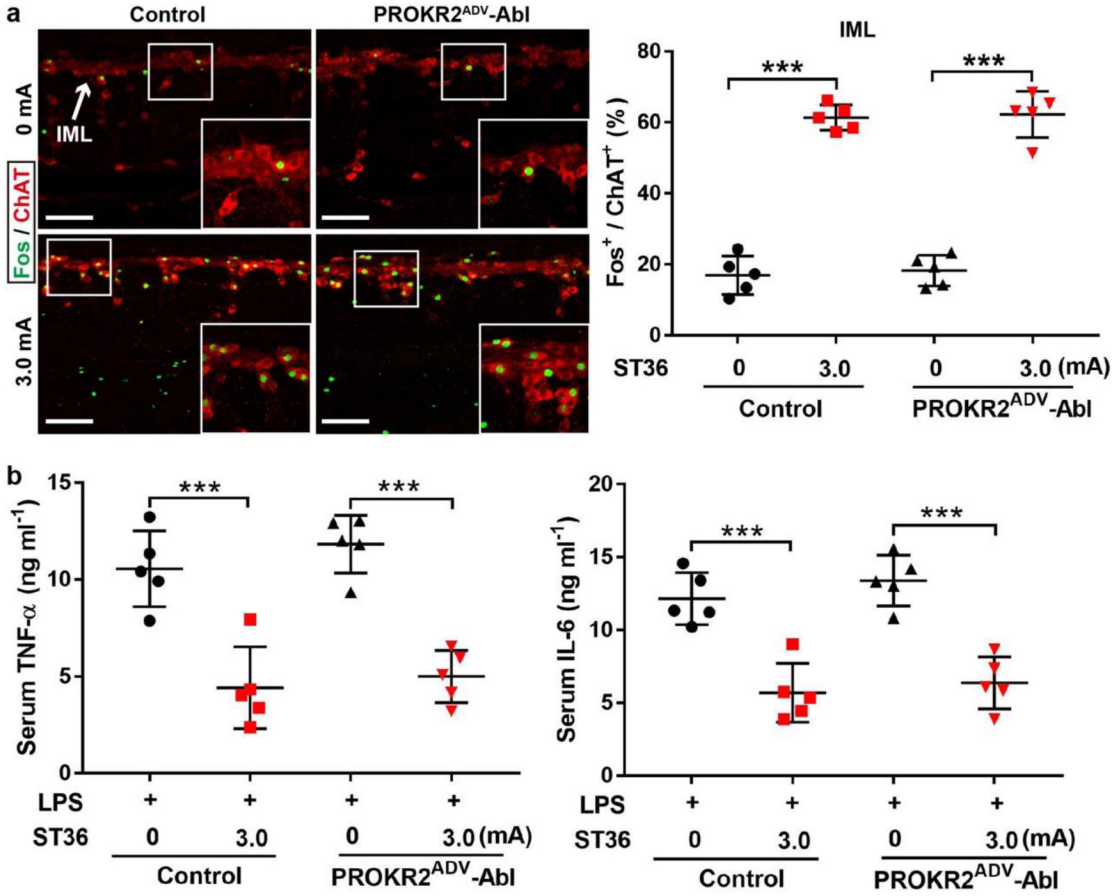

Extended Data Fig. 7. 3.0 mA ES of ST36 produced anti-inflammatory effects independent of PROKR2^{ADV} neurons.

a, Compared with control littermates, no difference of 3.0 mA ST36 ES-evoked Fos (green) induction in ChAT^{+} (red) sympathetic preganglionic neurons in the spinal intermediolateral nuclei ("IML") in PROKR2^{ADV}-Abl mice (two-way ANOVA, n = 5 mice per group, $F_{1, 16}$ = 0.236, P = 0.633; *post-hoc* Tukey's test: ***P < 0.001). **b,** No changes in 3.0 mA ST36 ES-evoked reduction of LPS-induced TNF-a and IL-6 production in PROKR2^{ADV}-Abl mice (two-way ANOVA, n = 5 mice per group; for TNF-a: $F_{1, 16}$ = 1.392, P = 0.255; *post-hoc* Tukey test: ***P < 0.001; for IL-6: $F_{1, 16}$ = 1.382, P = 0.257; *post-hoc* Tukey test: ***P < 0.001). Thus, although PROKR2^{ADV} neurons are necessary for low-intensity ES to drive the vagal-adrenal anti-inflammatory axis, they are dispensable for high-intensity ES to drive spinal-sympathetic anti-inflammatory axis from either ST25 or ST36. Data are shown as mean ± SEM. Scale bars: 100 μm.

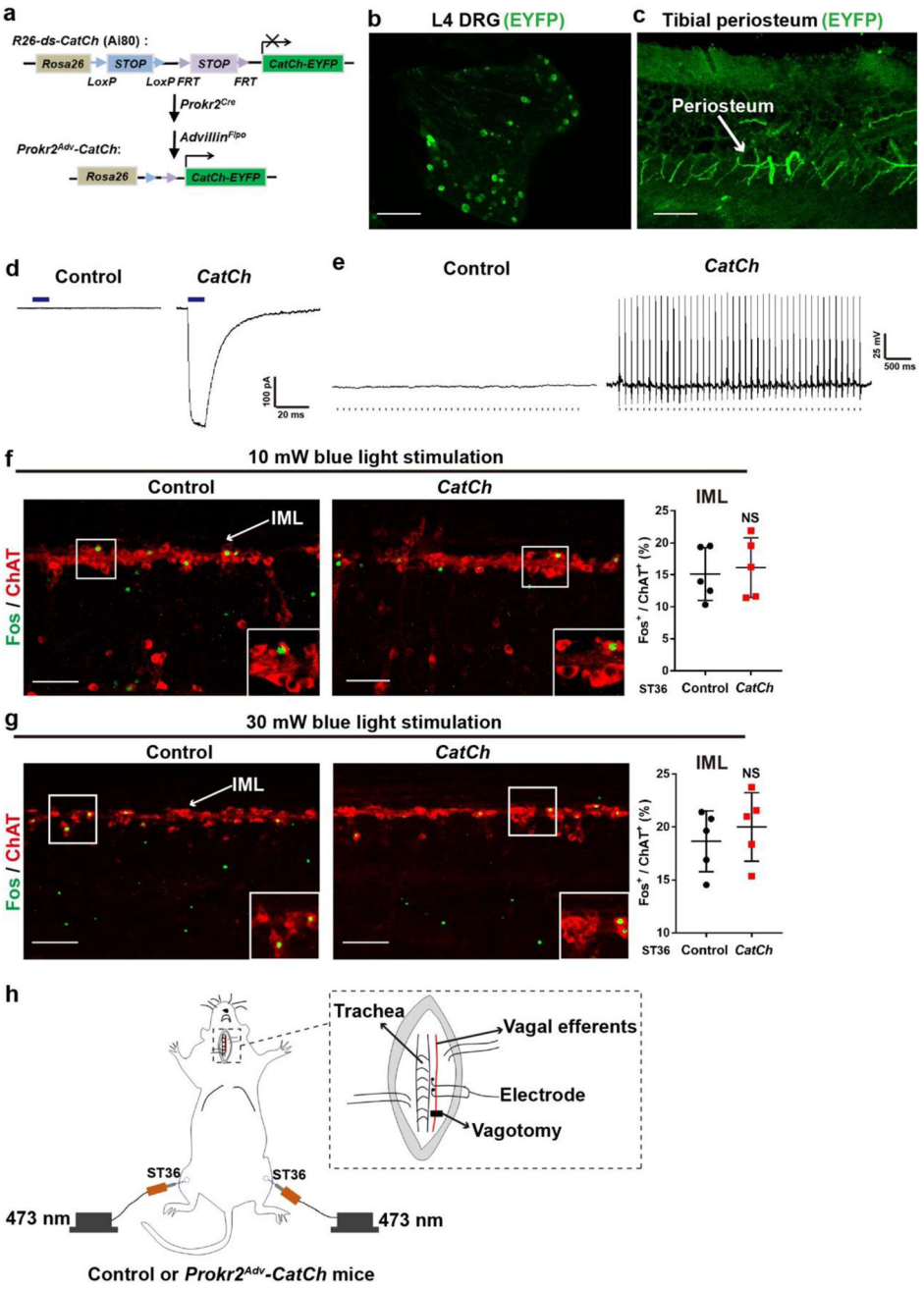

Extended Data Fig. 8. Optogenetic activation of PROKR2^{ADV} neurons inside the hindlimb ST36 region failed to drive sympathetic reflex.

a, Intersectional genetic strategy for generation of *Prokr2^{Adv}-CatCh* (or "*CatCh*") mice, in which the expression of the calcium translocating channelrhodopsin (CatCh, an L132C-mutated channelrhodopsin with enhanced Ca^{2+} permeability) plus the fluorescent protein EYFP was confined to PROKR2^{ADV} DRG neurons defined by co-expression of PROKR2^{Cre} and ADVILLIN^{Flpo}. This was achieved by crossing the intersectional *CatCh* mice (Ai80) with *Prokr2^{Cre}* and *Advillin^{Flpo}* mice. **b, c,** Representative images showing that CatCh-EYFP expression was detected in a subset of L4 DRG and EYFP^{+} fibers innervated tibial periosteum. n = 5 mice. **d, e,** Electrophysiological recordings of dissociated DRG

neurons from control and *CatCh* mice. Under the voltage clamp mode, blue light (473 nm) stimulation (10 Hz, 50 μs, 10 mW) resulted in inward currents in 26.3% (15/57) of randomly selected DRG neurons from *CatCh* mice (**d**), and after switching to the current clamp mode, this optical stimulation (10 Hz, 50 μs, 10 mW) reliably produced action potential firing (**e**). None of DRG neurons from control mice produced such inward currents and action potential firing (0/43 = 0%) (**d, e**). n = 3 mice per group. **f, g,** 10 mW (**f**) and 30 mW (**g**) optical stimulation of the hindlimb ST36 region in *CatCh* mice failed to produce an increase of Fos induction in $ChAT^+$ preganglionic sympathetic efferent neurons located in the spinal intermediolateral nuclei ("IML") compared to control mice (n = 5 mice per group, two-side student's unpaired *t*-test; for 10 mW: $t_8 = 0.362$; NS = not significant, $P = 0.727$; for 30 mW: $t_8 = 0.704$; NS, $P = 0.502$). **h,** Schematics showing how we recorded the left cervical vagal efferent nerve in response to 473 nm optic stimulation at bilateral ST36 sites in control and *CatCh* mice. Note that the distal end of the vagal nerve was transected to block visceral sensory afferent inputs. Data are shown as mean ± SEM. Scale bars: 100 μm.

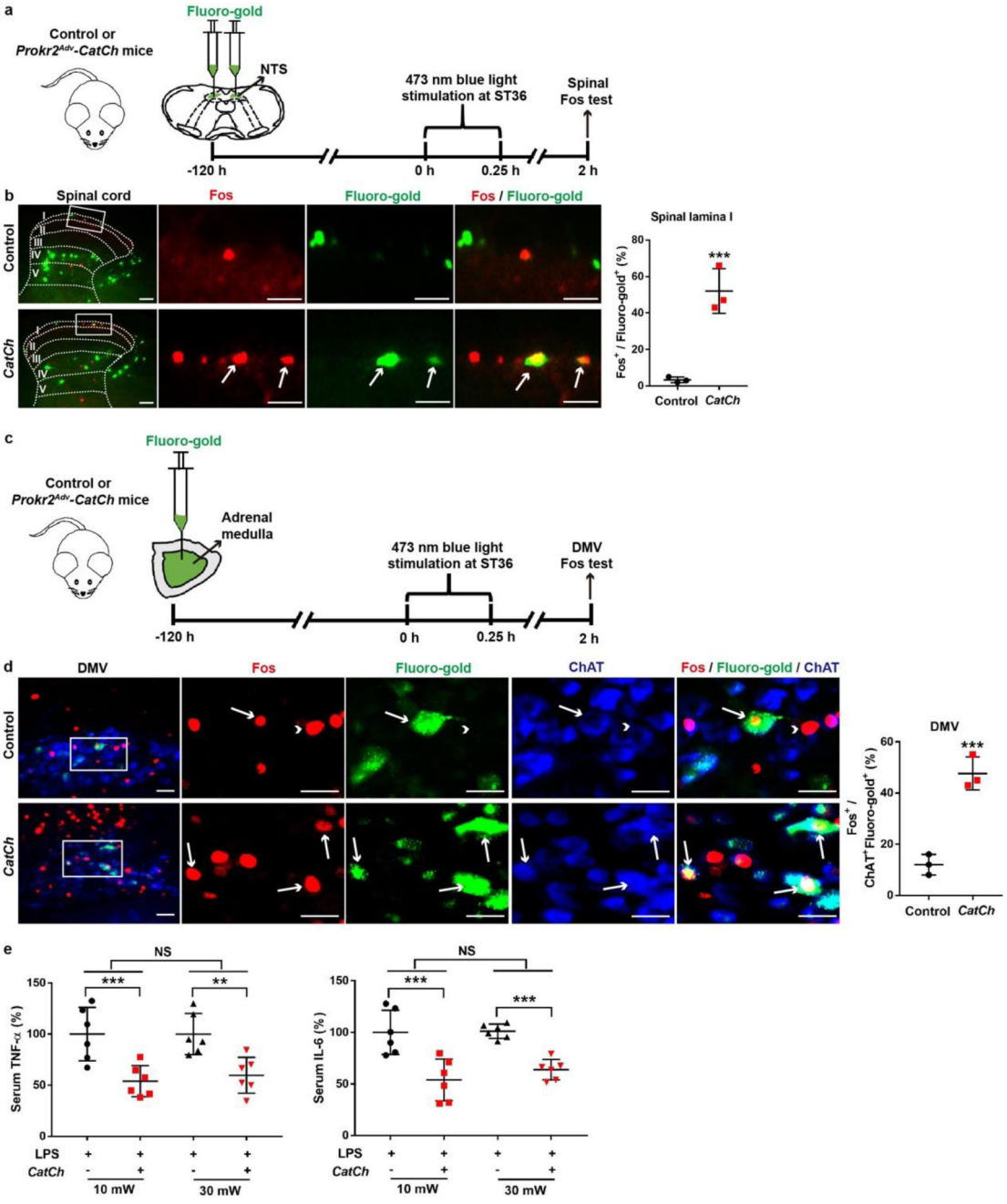

Extended Data Fig. 9. Optogenetic activation of hindlimb PROKR2^{ADV} neurons induced Fos in NTS-projecting spinal neurons and in adrenal medulla-projecting DMV efferent neurons.

a, Schematics showing the experimental design for testing if optical stimulation of PROKR2^{ADV} nerve fibers of the hindlimb ST36 region can activate spinal ascending projection neurons retrogradely labeled with Fluoro-gold from the nucleus tractus solitarius ("NTS") in hindbrain. **b,** 473 nm blue light stimulation of the hindlimb ST36 region was sufficient to evoke Fos induction in NTS-projecting neurons located in the lamina I of the spinal cord in *Prokr2^{Adv}-CatCh* ("*CatCh*") mice (**b**, arrows), but not in control mice (n = 3 mice per group, two-side student's unpaired *t*-test, $t_4 = 6.807$, $^{***}P < 0.001$). This

stimulation virtually did not induce any Fos in NTS-projecting neurons located in deep laminae (IV and V) of the spinal cord, in both control (1.77 ± 0.24%) and *CatCh* (2.27 ± 0.43%) mice (data not shown; n = 3 mice per group, two-side student's unpaired *t*-test, t_4 = 1.023, P = 0.364). **c,** Schematics showing the experimental design for testing if optical stimulation of PROKR2^{ADV} nerve fibers of the hindlimb ST36 region can activate a subset of vagal efferent neurons located in the dorsal motor nucleus of the vagus (DMV) that were retrogradely labeled from the adrenal gland with Fluoro-gold. **d,** Optical stimulation of PROKR2^{ADV} neurons of ST36 regions caused an increase in Fos induction in adrenal medulla-projecting DMV neurons compared with control mice (n = 3 mice per group, two-side student's unpaired *t*-test, t_4 = 8.159, ***P = 0.001). Arrows indicate retrogradely labeled DMV neurons with Fos induction. Arrowhead indicates the baseline Fos expression in ChAT-negative cells. **e,** No significant (NS) reduction of LPS-induced TNF-a and IL-6 production following 10 mW or 30 mW optical stimulation of PROKR2^{ADV} fibers at the ST36 site of *CatCh* mice compared with control mice (two-way ANOVA, n = 5 mice per group; for TNF-a: $F_{1, 20}$ = 0.124; NS, P = 0.728; *post-hoc* Tukey test: **P = 0.003, ***P < 0.001; for IL-6: $F_{1, 20}$ = 0.714; NS, P = 0.408; *post-hoc* Tukey test: ***P < 0.001). Data are shown as mean ± SEM. Scale bars: 100 μm.

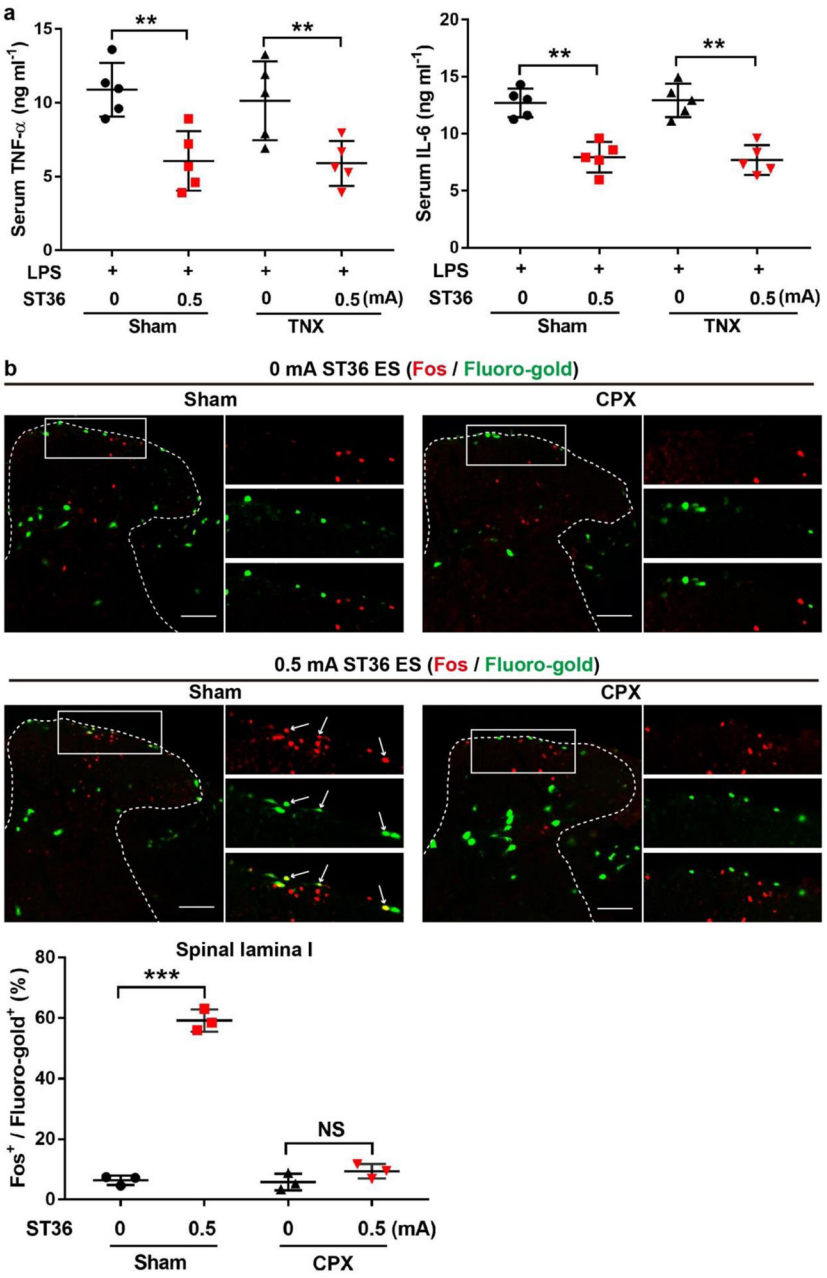

Extended Data Fig. 10. The tibial nerve was dispensable for focal 0.5 mA ST36 ES-evoked anti-inflammatory effects, and the common peroneal nerve was required for 0.5 mA ST36 ES to induce Fos in NTS-projecting spinal neurons.

a, 0.5 mA ST36 ES-evoked reduction of LPS-induced TNF-a and IL-6 in serum, compared with sham 0 mA ES, was unaffected by tibial nerve neurectomy ("TNX") compared with sham surgery ("sham") (two-way ANOVA, n = 5 mice per group; for TNF-α: $F_{1, 16} = 0.253$, $P = 0.622$; *post hoc* Tukey's test: left $^{**}P = 0.002$, right $^{**}P = 0.005$; for IL-6: $F_{1, 16} = 0.002$, $P = 0.989$; *post hoc* Tukey's test: left $^{**}P = 0.009$, right $^{**}P = 0.007$). As described in Extended data Fig. 3a, the tibial nerve was located posterior to fibula and tibia, and our focal ES of ST36 apparently failed to activate this nerve. This is different from reported activation of this nerve via a diffuse ES mode[10], in which the electric current entered the left ST36 site

and came out of the right ST36 site[10]. **b**, 0.5 mA, but not 0 mA control, ES of ST36 induced Fos (green) in Fluoro-gold$^+$ retrogradely labeled NTS-projecting neurons (red) located in the lamina I of the spinal cord in sham surgery mice, with arrows indicating co-labeling. This induction was lost in mice with common peroneal neurectomy ("CPX") (Two-way ANOVA, n = 3 mice per group, $F_{1,8} = 265.645$, $P < 0.001$; *post-hoc* Tukey's test: ***$P < 0.001$; NS, not significant, $P = 0.145$). Data are shown as mean ± SEM. Scale bars: 100 μm.

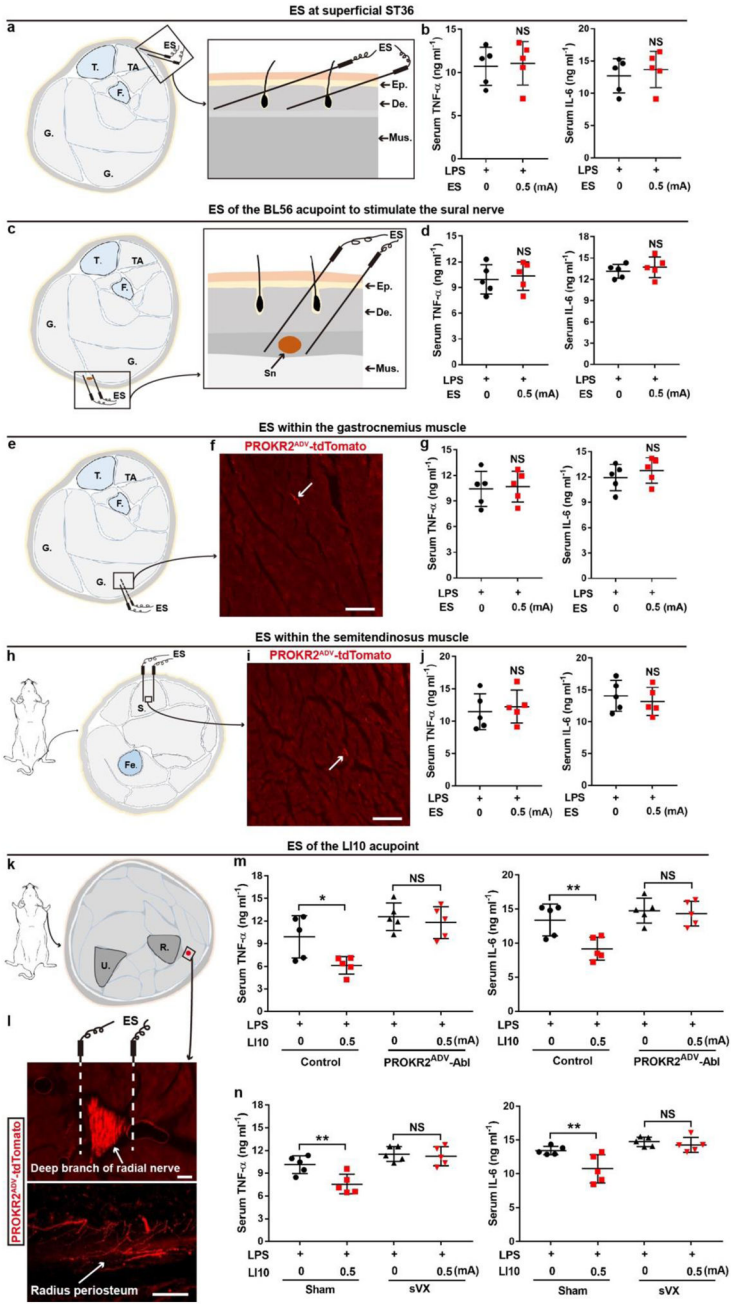

Extended Data Fig. 11. 0.5 mA ES at cutaneous or traditional non-acupoint regions failed to suppress inflammation, but ES at the forelimb LI10 acupoint can evoke PROKR2^{ADV} neuron-dependent anti-inflammatory effects.

a, b, low-intensity ES at the superficial ST36 region. Schematics (**a**) showing ES at the superficial, intradermal part of the ST36 region. Two electric needles were inserted through the epidermis ("Ep.") and into the dermis ("De.") at ST36 regions, with needles tilted to restrict them within the superficial dermis. This intradermal 0.5-mA ES failed to reduce LPS-induced TNF-a and IL-6 expression compared with sham 0 mA ES in C57BL/6J mice (**b**, n = 5 mice per group; two-side student's unpaired *t*-test; for TNF-a: $t_8 = 0.218$; NS, not significant, $P = 0.833$; for IL-6: $t_8 = 0.562$; NS, $P = 0.589$). **c, d,** Low-intensity stimulation of the sural nerve. Schematics (**c**) showing ES at the middle region of the posterior hind leg, by inserting electric needles through the Chengjin (BL56) acupoint, with tips flanking the skin-innervating sural nerve ("Sn"). 0.5 mA ES at this acupoint failed to reduce TNF-a and IL-6 compared with sham 0 mA ES in C57BL/6J mice (**d**, n = 5 mice per group; two-side student's unpaired *t*-test; for TNF-a: $t_8 = 0.375$; NS, $P = 0.718$; for IL-6: $t_8 = 0.721$; NS, $P = 0.491$). **e-j,** Low-intensity ES within the gastrocnemius ("G.") muscle or the semitendinosus ("S.") muscles. Schematics (**e, h**) showing ES at these two muscles. Two representative images (**f, i**) showing sparse innervation by PROKR2^{ADV}-tdTomato^{+} fibers within these muscles, with the percentages of unit areas showing positive fibers (0.51 ± 0.19% for G. and 0.60 ± 0.11% for S. muscles) comparable to that seen in the outer TA muscle (0.51 ± 0.15%) and the abdominal wall muscles (0.59 ± 0.12%) shown in Extended Data Fig. 4h. n = 4 mice. In comparison with sham 0 mA ES, no impact on TNF-a and IL-6 production by 0.5 mA ES in either G. muscle (**g**, n = 5 mice per group. two-side student's unpaired *t*-test; for TNF-a: $t_8 = 0.205$; NS, $P = 0.843$; for IL-6: $t_8 = 0.861$; NS, $P = 0.415$) or in S. mucle (**j**, n = 5 mice per group; two-side student's unpaired *t*-test; for TNF-a: $t_8 = 0.468$; NS, $P = 0.652$; for IL-6: $t_8 = 0.593$; NS, $P = 0.570$) in C57BL/6J mice. **k-m,** Low-intensity ES at the forelimb acupoint LI10 (Shousanli). Schematics (**k**) and the image (**l**, top) showing ES at the forelimb acupoint LI10. Representative images (**l**) showing PROKR2^{ADV}-tdTomato^{+} fibers within the deep branch of the radial nerve, and their innervations in radius periosteum, which were prominent at transverse sections at levels slightly distal (e.g., 1 mm) from the LI10 acupoint level. n = 3 mice. (**m**) Loss of 0.5 mA LI10 ES-evoked reduction of TNF-a and IL-6 in PROKR2^{ADV}-Abl mice compared with control mice (two-way ANOVA, n = 5 mice per group; for TNF-a: $F_{1, 16} = 20.384$, $P < 0.001$; *post-hoc* Tukey test: $^{*}P = 0.011$; NS, $P = 0.562$; for IL-6: $F_{1, 16} = 14.296$, $P = 0.002$; *post-hoc* Tukey test: $^{**}P = 0.004$; NS, $P = 0.728$). (**n**) Loss of 0.5 mA LI10 ES-evoked reduction of TNF-a and IL-6 in mice with subdiaphragmatic vagotomy ("sVX") compared with mice with sham surgery (two-way ANOVA, n = 5 mice per group; for TNF-a: $F_{1, 16} = 22.875$, $P < 0.001$; *post-hoc* Tukey test: $^{**}P = 0.004$; NS, $P = 0.697$; for IL-6: $F_{1, 16} = 18.065$, $P = 0.002$; *post-hoc* Tukey test: $^{**}P = 0.004$; NS, $P = 0.57$). TA: Anterior tibial muscle; T.: Tibia; F.: Fibula; Fe.: Femur; R.: Radius; U.: Ulna. Data are shown as mean ± SEM. Scale bars: 100 μm.

Acknowledgements

We thank D. D. Ginty for critical comments, and W. Lu and B. Zhao for helpful discussions; D. D. Ginty, M. Goulding, S. M. Dymecki, staff at GENSAT/MMRRC at the University of Davis, and the Allen Brain Institute/the Jackson Laboratory for genetically modified mice; and S. Celine for her assistance in histochemical analyses. All experimental data were generated at the Dana-Farber Cancer Institute, and the work was supported primarily by a NIH grant (R01AT010629) and partially by the Harvard/MIT Joint Research Program in Basic Neuroscience and a Wellcome Trust grant (200183/Z/15/Z) to Q.M. S.L.'s salary was supported primarily by a NIH grant (R01AT010629) and partly by the China Postdoctoral Science Foundation (KLF101846) and by the Development Project of Shanghai Peak Disciplines-Integrated Medicine (20150407) during an early period before

the NIH grant (R01AT010629) was funded. Y.S.'s and W.Y.'s salary was supported by the China Scholarship Council (CSC no. 201609110039 and CSC no. 20190600178, respectively). Z.W.'s salary was supported by Fujian University of Traditional Chinese Medicine and by the Harvard/MIT Joint Research Program in Basic Neuroscience. Histochemical imaging was supported by Boston Children's Hospital IDDRC (1U54HD090255).

Data availability

All data are included in the paper and available from the corresponding author upon request. Source data are provided with this paper.

References

1. Kametani H, Sato A, Sato Y & Simpson A Neural mechanisms of reflex facilitation and inhibition of gastric motility to stimulation of various skin areas in rats. J. Physiol 294, 407–418 (1979). [PubMed: 512950]
2. Sato A & Schmidt RF The modulation of visceral functions by somatic afferent activity. Jpn. J. Physiol 37, 1–17 (1987). [PubMed: 3302431]
3. Sato A Neural mechanisms of autonomic responses elicited by somatic sensory stimulation. Neurosci. Behav. Physiol 27, 610–621 (1997). [PubMed: 9353786]
4. Li YQ, Zhu B, Rong PJ, Ben H & Li YH Neural mechanism of acupuncture-modulated gastric motility. World J. Gastroenterol 13, 709–716 (2007). [PubMed: 17278193]
5. Takahashi T Effect and mechanism of acupuncture on gastrointestinal diseases. Int. Rev. Neurobiol 111, 273–294 (2013). [PubMed: 24215928]
6. Ma Q Somato–autonomic reflexes of acupuncture. Med. Acupunct 32, 362–366 (2020). [PubMed: 33362888]
7. Chavan SS, Pavlov VA & Tracey KJ Mechanisms and therapeutic relevance of neuro-immune communication. Immunity 46, 927–942 (2017). [PubMed: 28636960]
8. Ulloa L, Quiroz-Gonzalez S & Torres-Rosas R Nerve stimulation: immunomodulation and control of inflammation. Trends Mol. Med 23, 1103–1120 (2017). [PubMed: 29162418]
9. Pan WX, Fan AY, Chen S & Alemi SF Acupuncture modulates immunity in sepsis: toward a science-based protocol. Auton. Neurosci 232, 102793 (2021). [PubMed: 33684727]
10. Torres-Rosas R et al. Dopamine mediates vagal modulation of the immune system by electroacupuncture. Nat. Med 20, 291–295 (2014). [PubMed: 24562381]
11. Liu S et al. Somatotopic organization and intensity dependence in driving distinct NPY-expressing sympathetic pathways by electroacupuncture. Neuron 108, 436–435 (2020). [PubMed: 32791039]
12. Longhurst JC Defining meridians: a modern basis of understanding. J. Acupunct. Meridian Stud 3, 67–74 (2010). [PubMed: 20633518]
13. Yang FC et al. Genetic control of the segregation of pain-related sensory neurons innervating the cutaneous versus deep tissues. Cell Rep. 5, 1353–1364 (2013). [PubMed: 24316076]
14. Choi S et al. Parallel ascending spinal pathways for affective touch and pain. Nature 587, 258–263 (2020). [PubMed: 33116307]
15. Zylka MJ, Rice FL & Anderson DJ Topographically distinct epidermal nociceptive circuits revealed by axonal tracers targeted to *Mrgprd*. Neuron 45, 17–25 (2005). [PubMed: 15629699]
16. Ghitani N et al. Specialized mechanosensory nociceptors mediating rapid responses to hair pull. Neuron 95, 944–954.e4 (2017). [PubMed: 28817806]
17. Sharma N et al. The emergence of transcriptional identity in somatosensory neurons. Nature 577, 392–398 (2020). [PubMed: 31915380]
18. Kupari J et al. Single cell transcriptomics of primate sensory neurons identifies cell types associated with chronic pain. Nat. Commun 12, 1510 (2021). [PubMed: 33686078]
19. Kucera J & Walro JM An immunocytochemical marker for early type I muscle fibers in the developing rat hindlimb. Anat. Embryol. (Berl.) 192, 137–147 (1995). [PubMed: 7486010]

20. Remick DG, Newcomb DE, Bolgos GL & Call DR Comparison of the mortality and inflammatory response of two models of sepsis: lipopolysaccharide vs. cecal ligation and puncture. Shock 13, 110–116 (2000). [PubMed: 10670840]
21. Kleinlogel S et al. Ultra light-sensitive and fast neuronal activation with the Ca^{2+}-permeable channelrhodopsin CatCh. Nat. Neurosci 14, 513–518 (2011). [PubMed: 21399632]
22. Lima D in The Senses: A Comprehensive Reference Vol. 5 (eds Masland RH et al.) 477–526 (Academic, 2008).
23. Travagli RA & Anselmi L Vagal neurocircuitry and its influence on gastric motility. Nat. Rev. Gastroenterol. Hepatol 13, 389–401 (2016). [PubMed: 27251213]
24. Damarey B et al. Imaging of the nerves of the knee region. Eur. J. Radiol 82, 27–37 (2013). [PubMed: 21596499]
25. Quiroz-Gonzalez S, Segura-Alegria B, Guadarrama-Olmos JC & Jimenez-Estrada I Cord dorsum potentials evoked by electroacupuncture applied to the hind limbs of rats. J. Acupunct. Meridian Stud 7, 25–32 (2014). [PubMed: 24513345]
26. Peng Z, Nan G, Cheng M & Zhou K The comparison of trigger point acupuncture and traditional acupuncture. World J. Acupunct. Moxibustion 26, 1–6 (2016).
27. Choi EM, Jiang F & Longhurst JC Point specificity in acupuncture. Chin. Med 7, 4 (2012). [PubMed: 22373514]
28. Xing JJ, Zeng BY, Li J, Zhuang Y & Liang FR Acupuncture point specificity. Int. Rev. Neurobiol 111, 49–65 (2013). [PubMed: 24215917]
29. Langevin HM & Wayne PM What is the point? The problem with acupuncture research that no one wants to talk about. J. Altern. Complement. Med 24, 200–207 (2018). [PubMed: 29493256]
30. van der Poll T, van de Veerdonk FL, Scicluna BP & Netea MG The immunopathology of sepsis and potential therapeutic targets. Nat. Rev. Immunol 17, 407–420 (2017). [PubMed: 28436424]
31. Gerfen CR, Paletzki R & Heintz N GENSAT BAC Cre-recombinase driver lines to study the functional organization of cerebral cortical and basal ganglia circuits. Neuron 80, 1368–1383 (2013). [PubMed: 24360541]
32. Bourane S et al. Identification of a spinal circuit for light touch and fine motor control. Cell 160, 503–515 (2015). [PubMed: 25635458]
33. Liu Y et al. VGLUT2-dependent glutamate release from peripheral nociceptors is required to sense pain and suppress itch. Neuron 68, 543–556 (2010). [PubMed: 21040853]

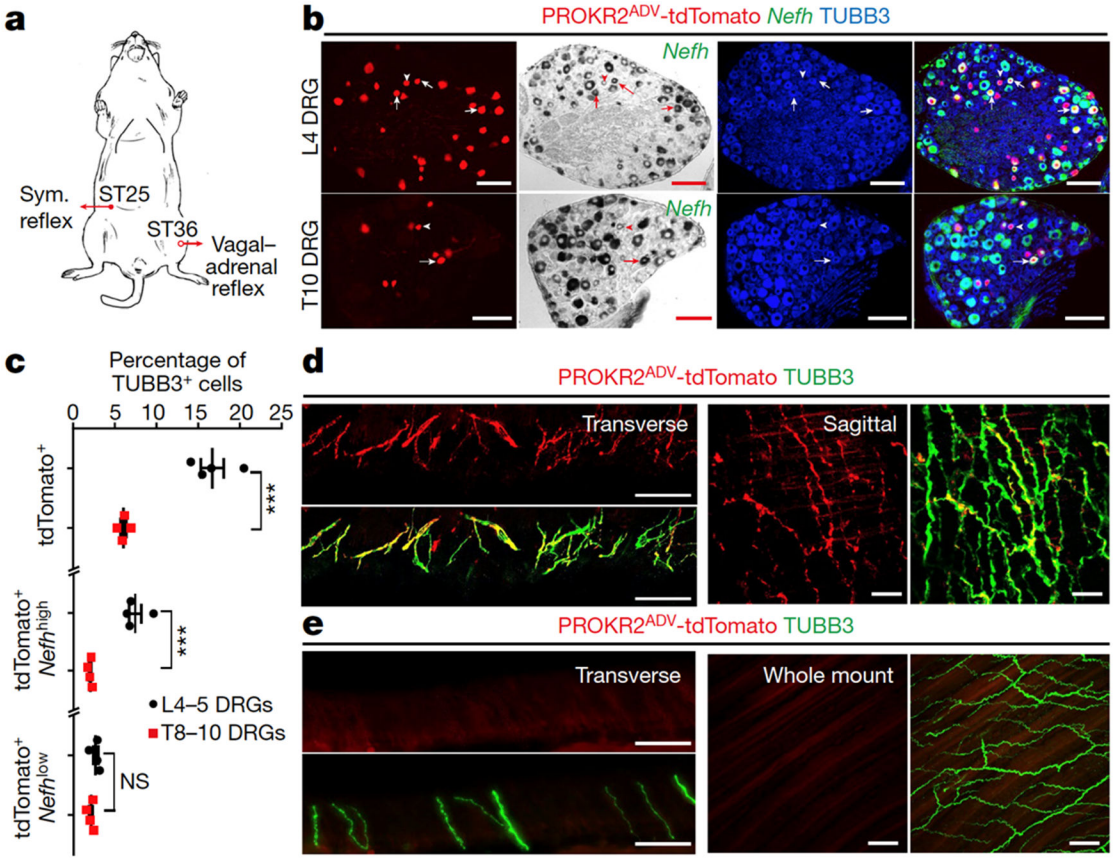

Fig. 1: Characterizing PROKR2^{ADV} neurons.

a, Schematic of the somatotopic organization that drives two autonomic pathways by ES. Sym., sympathetic. **b,** Sections through L4–L5 and T8–T10 DRGs from *Prokr2^{Adv}-tdTomato* mice showing the colocalization of tdTomato (red) with *Nefh* mRNA expression (bright-field images converted to pseudo-green in merged images) and the pan-neuronal marker TUBB3 (blue). Arrows and arrowheads indicate tdTomato^{+} neurons with high and low levels of *Nefh* mRNA expression, respectively. n = 4 mice. **c,** The percentage of TUBB3^{+} neurons expressing the indicated markers in L4–L5 and T8–T10 DRGs (n = 4 mice; two-sided Student's unpaired *t*-test; for tdTomato^{+}, $t_6 = 7.512$, ***$P < 0.001$; for tdTomato^{+}*Nefh*^{high}, $t_6 = 7.201$, ***$P < 0.001$; for tdTomato^{+}*Nefh*^{low}, $t_6 = 1.714$, not significant (NS), $P = 0.137$). **d, e,** Transverse and sagittal sections through the tibial bone periosteum (**d**), and transverse sections plus whole-mount preparation of the abdominal peritoneum (**e**) from adult *Prokr2^{Adv}-tdTomato* mice showing tdTomato (red) and TUBB3 (green) localization. n = 5 mice. Scale bars, 100 μm. Data are mean ± s.e.m.

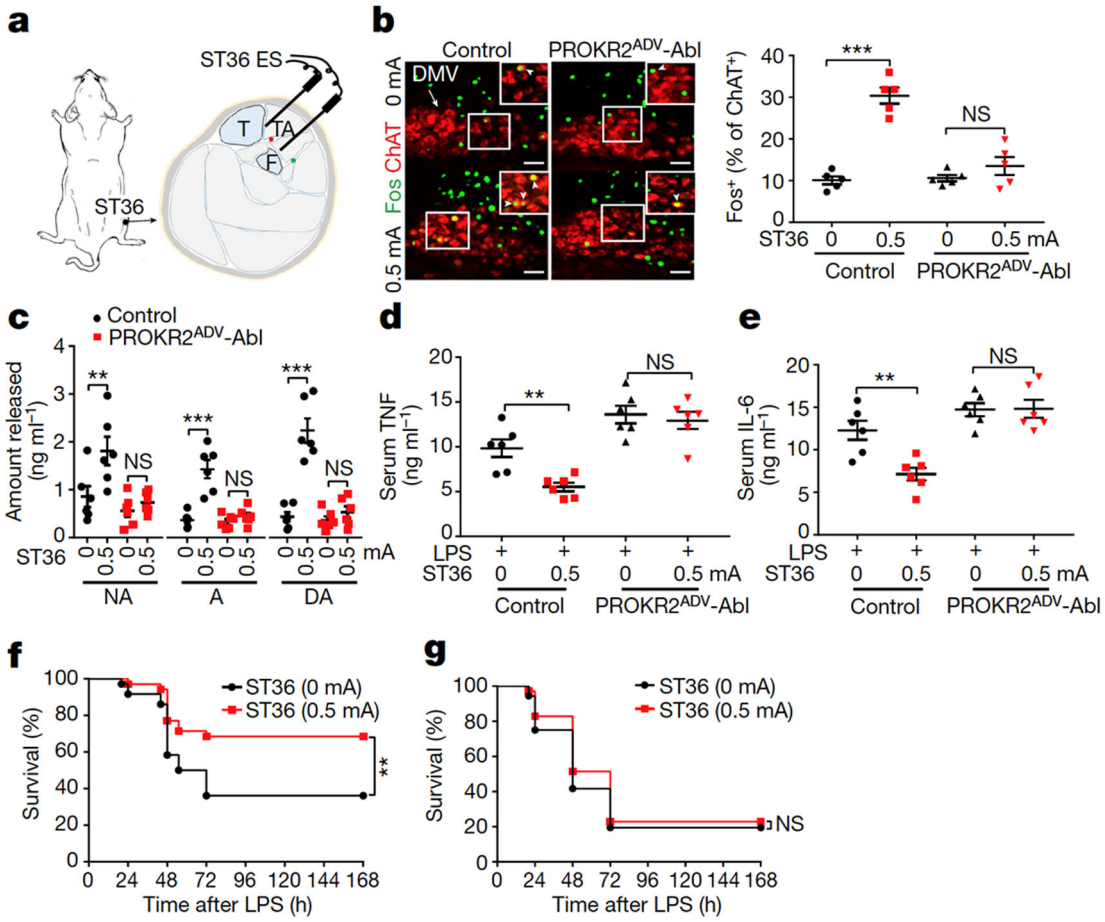

Fig. 2: Requirement of PROKR2^{ADV} neurons for low-intensity ES to drive the vagal–adrenal anti-inflammatory axis.

a, Schematic of ES at the ST36 site. The red and green dots close to the needle tips represent the deep and superficial branches, respectively, of the peroneal nerve. F, fibula; T, tibia. **b,** Images (left) and quantification (right) of Fos expression (green) induced by ES (0.5 mA) at the ST36 acupoint in ChAT^{+} (red) DMV neurons in control but not in PROKR2^{ADV}-Abl mice. Two-way ANOVA, n = 5 mice, $F_{1, 16} = 26.769$, $P < 0.001$; *post hoc* Tukey's test: ***$P < 0.001$; NS, $P = 0.204$. Arrow, ChAT^{+} cells in DMV; arrowheads, Fos^{+}ChAT^{+} neurons. **c,** ES (0.5 mA) at the ST36 site increased the release of noradrenaline (NA), adrenaline (A) and dopamine (DA) in control but not PROKR2^{ADV}-Abl mice. Two-way ANOVA, n = 6 mice, $F_{1, 20} = 11.603$ (NA), 21.338 (A), 33.220 (DA), $P < 0.001$; *post hoc* Tukey test: ***$P < 0.001$; NS, $P = 0.535$ (NA), 0.487 (A) and 0.450 (DA). **d, e,** PROKR2^{ADV}-Abl mice exhibited loss of 0.5-mA ES ST36-evoked TNF (**d**) and IL-6 (**e**) anti-inflammatory effects compared with control mice. Two-way ANOVA, n = 6 mice; for TNF: $F_{1, 20} = 40.025$, $P < 0.001$; *post hoc* Tukey test: **$P = 0.003$; NS, $P = 0.596$; for IL-6: F1, 20 = 28.573, $P < 0.001$; *post hoc* Tukey test: **$P = 0.002$; NS, $P = 0.931$. **f, g,** ES (0.5 mA) at the ST36 site (compared with 0 mA ES) increased survival rates in LPS-treated control mice (**f**; two-sided log-rank test, **$P = 0.008$) but not in PROKR2^{ADV}-Abl mice (**g**; two-sided log-rank test, NS, $P = 0.456$). n = 36 (0 mA) or 35 (0.5 mA) mice. Scale bars, 100 μm. Data are mean ± s.e.m.

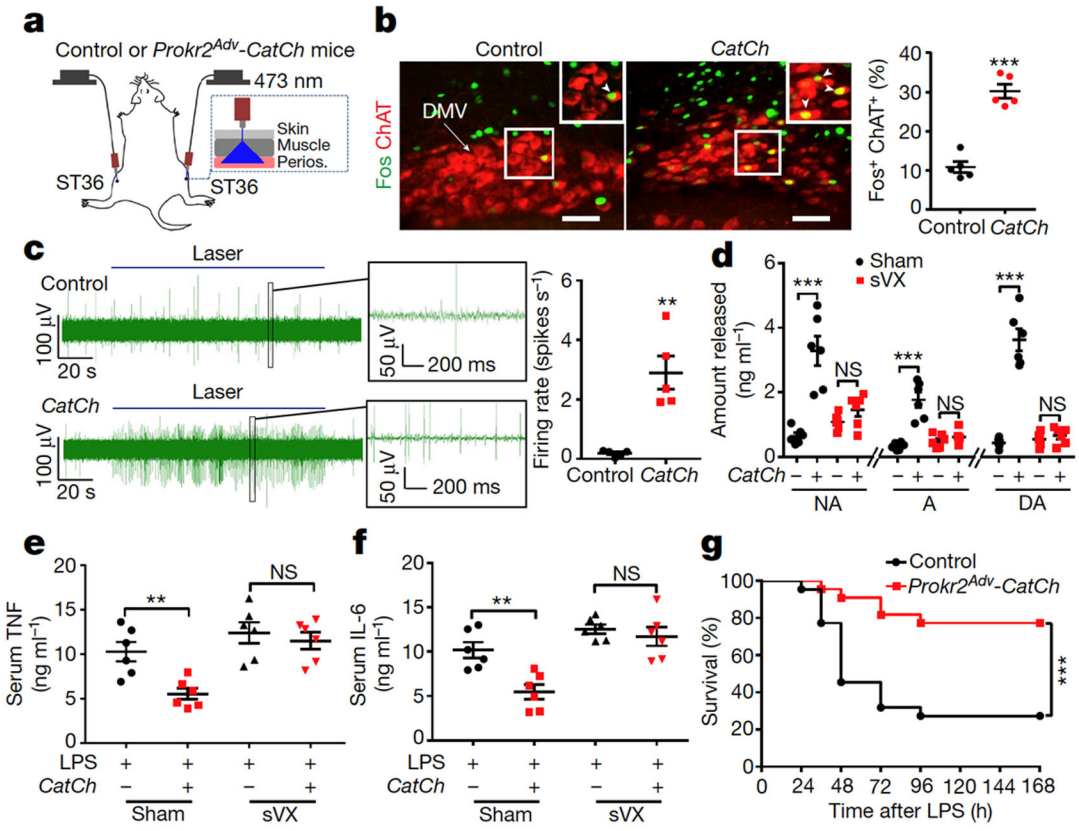

Fig. 3: Activation of PROKR2^{ADV} fibres drives the vagal–adrenal anti-inflammatory axis.

a, Schematic of optical stimulation of the ST36 acupoint in control and *Prokr2^{Adv}-CatCh* (*CatCh*) mice. Perios, periosteum. **b,** Images (left) and quantification (right) of Fos (green) induction in ChAT^{+} (red) DMV neurons (n = 5 mice; two-sided Student's unpaired *t*-test, t_8 = 8.713, ***P < 0.001). Arrow, ChAT^{+} cells in DMV; arrowheads, Fos^{+}ChAT^{+} neurons. **c,** Left, example vagal efferent electrical activity traces from *CatCh* and control mice. Right, *CatCh* mice exhibit increased firing compared with control mice (n = 5 mice per group; two-sided Student's unpaired *t*-test, t_8 = 4.855, **P = 0.001). **d,** *CatCh* mice show loss of increased release of noradrenaline, adrenaline and dopamine induced by optical activation of PROKR2^{ADV} fibres following subdiaphragmatic vagotomy (sVX) compared with mice that underwent sham surgery. Two-way ANOVA, n = 6 mice, $F_{1, 20}$ = 33.278 (NA), 33.188 (A), 80.020 (DA), P < 0.001; *post hoc* Tukey's paired comparisons: ***P < 0.001; NS, P = 0.326 (NA), P = 0.584 (A) and P = 0.697 (DA). – denotes control littermates and + denotes *CatCh* mice. **e, f,** Optical activation of PROKR2^{ADV} fibres reduced LPS-induced production of TNF (**e**) and IL-6 (**f**) in mice that underwent sham surgery but not in sVX mice. Two-way ANOVA, n = 6 mice; for TNF: $F_{1, 20}$ = 8.021, P < 0.001; for IL-6: $F_{1, 20}$ = 10.695, P = 0.004; *post hoc* Tukey's test: **P = 0.003 (TNF) or P = 0.001 (IL-6); NS, P = 0.535 (TNF) or P = 0.486 (IL-6). **g,** Optical activation of PROKR2^{ADV} fibres promoted survival in *CatCh* mice (n = 22 mice per group, two-sided log-rank test, ***P < 0.001). Scale bars, 100 µm. Data are mean ± s.e.m.

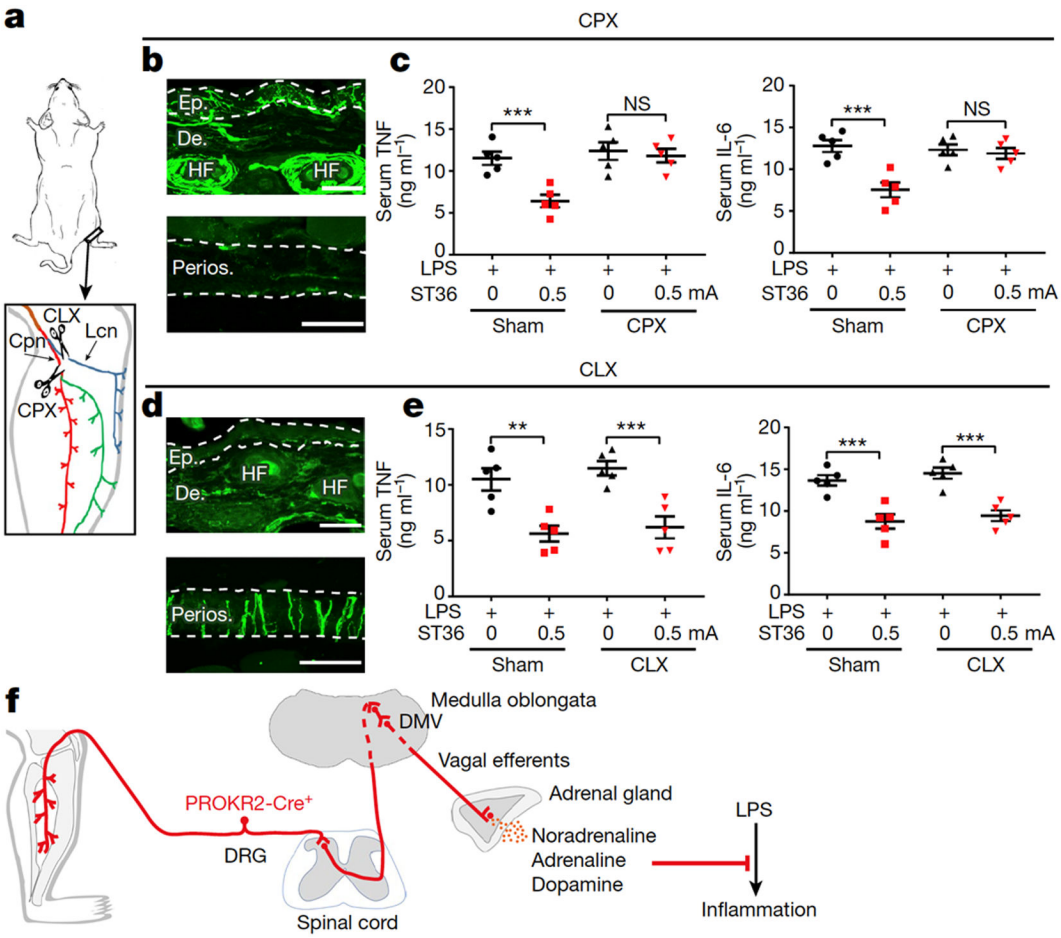

Fig. 4: Requirement of deep-tissue-innervating nerves for anti-inflammatory effects.

a, Schematic of common peroneal nerve (Cpn) neurectomy (CPX) and lateral cutaneous nerve (Lcn) neurectomy (CLX). **b,** CPX mice showed preservation of TUBB3^{+} fibres (green) in the epidermis (Ep.) and dermis (De.) of skin at the ST36 region (top), but loss in the tibial periosteum (the anterior side; bottom). HF, hair follicle. n = 3 mice. **c,** ES (0.5 mA) at ST36 reduced LPS-induced production of TNF (left) and IL-6 (right) in mice that underwent sham surgery compared with CPX. Two-way ANOVA, n = 5 mice; for TNF, $F_{1,\,16} = 13.653$, $P = 0.002$; for IL-6: $F_{1,\,16} = 6.917$, $P = 0.018$; *post hoc* Tukey's test: ***$P <$ 0.001; NS, $P = 0.652$ for TNF and $P = 0.687$ for IL-6. **d,** CLX mice showed loss of TUBB3^{+} nerve fibres (upper panel) in the skin at the ST36 site (top), but not in tibial periosteum (bottom). n = 3 mice. **e,** There were no changes in ES-evoked reduction of LPS-induced production of TNF (left) and IL-6 (right) in mice that underwent CLX compared with sham surgery. Two-way ANOVA, n = 5 mice; for TNF: $F_{1,\,16} = 0.843$, $P = 0.372$; for IL-6: $F_{1,\,16} = 1.229$, $P = 0.284$; *post hoc* Tukey's test: **$P = 0.001$, ***$P < 0.001$. **f,** Schematic of the vagal–adrenal axis driven by PROKR2^{Cre} neurons innervating deep limb fascial tissues. Scale bars, 100 μm. Data are mean ± s.e.m.